«ФИЗИКА ЭЛЕМЕНТАРНЫХ ЧАСТИЦ И АТОМНОГО ЯДРА»
2000, ТОМ 31, ВЫП. 4

УДК 539.1

DIPOLE EXCITATIONS IN DEFORMED NUCLEI

V.G. Soloviev, *A.V. Sushkov, N.Yu. Shirikova*

Joint Institute for Nuclear Research, Dubna

«ФИЗИКА ЭЛЕМЕНТАРНЫХ ЧАСТИЦ И АТОМНОГО ЯДРА»
2000, ТОМ 31, ВЫП. 4

УДК 539.1

DIPOLE EXCITATIONS IN DEFORMED NUCLEI

V.G. Soloviev, *A.V. Sushkov*, *N.Yu. Shirikova*

Joint Institute for Nuclear Research, Dubna

A study of the magnetic and electric dipole excitations is carried out within the quasiparticle–phonon nuclear model with the wave functions consisting of one- and two-phonon terms and in random-phase approximation for the deformed nuclei ^{154}Sm, ^{166,168}Er, ^{172,174}Yb, ^{178}Hf, and ^{238}U. It is shown that computed $M1$ strength below 4 MeV is much stronger fragmented than in Gd and Dy isotopes. The calculated $M1$ and $E1$ strengths summed in the energy range 2–4 MeV are in agreement with the relevant experimental data. It is found that the orbital motion, though giving on the whole a modest contribution to the $M1$ strength, plays a significant role in shaping the $M1$ spectra because of the destructive interference between orbital and spin amplitudes. Strong $E1$ transitions also occur in the same energy range. Their total strength in the energy range 3.6–7.6 MeV is about 4 times larger than the M1 strength. Because of these highly intense $E1$ transitions, the total dipole strength distribution computed as a sum of the $M1$ and $E1$ strengths is considerably different from the spectra of the $M1$ transitions alone.

Изучение магнитных и электрических дипольных возбуждений выполнено в рамках квазичастично-фононной модели с волновыми функциями, содержащими одно- и двухфононные члены, и в приближении хаотических фаз для деформированных ядер ^{154}Sm, ^{166,168}Er, ^{172,174}Yb, ^{178}Hf и ^{238}U. Показано, что рассчитанная $M1$-сила ниже 4 МэВ более расфрагментирована, чем для изотопов Gd и Dy. Рассчитанные $M1$- и $E1$-силы, просуммированные в интервале 2–4 МэВ, находятся в согласии с экспериментальными данными. Обнаружено, что орбитальное движение, дающее в целом небольшой вклад в распределение $M1$-силы, играет существенную роль в форме $M1$-спектра из-за деструктивной интерференции орбитальной и спиновой амплитуд. Сильные $E1$-переходы имеют место в этой же энергетической области. Полная сила их в интервале энергий 3,6–7,6 МэВ почти в 4 раза больше, чем $M1$-сила. Из-за этих очень сильных $E1$-переходов полное распределение дипольной силы, рассчитанное как сумма $M1$- и $E1$-сил, существенно отличается от спектра $M1$-переходов.

1. INTRODUCTION

A long series of experiments devoted to the study of the low-lying $M1$ excitations in deformed nuclei, first discovered in (e, e')-scattering experiments [1] and known as scissors mode [2], has led not only to an almost complete characterization of the mode but also to new interesting findings [3, 4]. Nuclear resonance fluorescent (NRF) experiments using polarized photons carried out for a systematic study of the dipole spectra in a large number of deformed heavy nuclei have established the existence of $E1$ levels mingled with $M1$ excitations in the same energy range 2–4 MeV (see [4] and references therein).

The low-lying $M1$ transitions have been intensively studied in a very large variety of theoretical approaches (see Ref. [5] for a review and references). However, a comprehensive microscopic study of both $M1$ and $E1$ spectra in this low-energy region has been carried out only within the quasiparticle–phonon nuclear model (QPNM). This approach extends the RPA formalism by treating a Hamiltonian of general separable form in a space spanned by one- and two-phonon states [6,7]. The calculations performed in this context produced $M1$ strengths of the right magnitude distributed over several peaks comparable in number to the ones found experimentally [8–10]. Analogous calculations have produced in the same energy region enhanced $E1$ transitions of comparable decay widths [9–11]. The enhancement of these $E1$ transitions has been found to be induced by the octupole–octupole interaction. Indeed, a close correlation between $E1$ and $E3$ transitions in this region has been found [12].

Proton scattering experiments, adopted originally to confirm the orbital nature of the low-lying $M1$ excitations [13, 14], were subsequently extended to higher energy [15]. These new measurements gave strong indications for the existence of spin $M1$ spectra in deformed rare earth nuclei like ^{154}Sm, ^{158}Gd, and ^{168}Er [15, 16] and in ^{238}U [17]. The strength is distributed over the energy interval 6–10 MeV and exhibits a double-humped structure. This peculiar shape is specially evident in ^{154}Sm, where two distinct wide peaks are visible at ~ 6 MeV and ~ 8 MeV, respectively. More recently, highly sensitive NRF experiments using a EUROBALL cluster module have been carried out at $E_0 = 7$ MeV to search for spin magnetic dipole strength in ^{154}Sm [18]. The dipole strength derived from the (γ, γ') experiment falls very rapidly to zero above 6 MeV. Such a deep minimum, not present in the (p, p') spectrum, may be explained with an extreme fragmentation of the strength and (or) a destructive interference between orbital and spin contributions. Another new feature of the (γ, γ') spectrum is the presence of non-negligible dipole strength, not seen in (p, p'), between 4–5 MeV. The detection of this unexpected strength may be a signal for the occurrence of $E1$ transitions in this region. Such a possibility is suggested by the fact, pointed out already, that $E1$ levels admixed with the orbital $M1$ excitations occur already in the low-energy region 2–4 MeV. The calculation of the $M1$ strength distribution in the energy range 4–12 MeV for the rare-earth nuclei ^{154}Sm, ^{168}Er, ^{178}Hf and for ^{238}U [19] was carried out in random-phase approximation (RPA). The same Hamiltonian, of general separable form, used in the QPNM with all parameters fixed in previous calculations by a fit of some low-lying levels was adopted. The calculation was therefore parameter free.

The aim of this review is to describe the results of calculation of the $M1$- and $E1$-strength distribution in ^{154}Sm, ^{166,168}Er, ^{172,174}Yb, ^{178}Hf, and ^{238}U in the low-lying and intermediate energy regions. This paper is organized as follows. In Sect. 2 we briefly describe the QPNM. A systematics of the results of calculations within the QPNM and comparison with the relevant experimental data and discussion are presented in Sect. 3. Dipole strength disrtibution at 4–12 MeV energy region is given in Sect. 4. Conclusions are drawn in the final Section 5.

2. QUASIPARTICLE-PHONON NUCLEAR MODEL

The initial QPNM Hamiltonian contains the average field of a neutron and a proton system in the form of the axial-symmetric Woods–Saxon potential, monopole pairing, isoscalar and isovector particle–hole (ph), as well as particle–particle (pp) multipole, spin-multipole and tensor interactions between quasiparticles. The effective interactions between quasiparticles are expressed as a series of multipoles and spin-multipoles. It is essential that the interaction between quasiparticles is presented in a separable form. In this paper, we used only the multipole and spin–spin interactions.

We now transform the initial QPNM Hamiltonian. For this purpose we perform a canonical Bogoliubov transformation

$$a_{q\sigma} = u_q \alpha_{q\sigma} + \sigma v_q \alpha^+_{q-\sigma} \tag{1}$$

in order to replace the particle operators $a_{q\sigma}$ and $a^+_{q\sigma}$ by the quasiparticle operators $\alpha_{q\sigma}$ and $\alpha^+_{q\sigma}$. We introduce the phonon operators of two types. If we take into account only interactions of the electric type, the phonon creation operator has the following standard form:

$$Q^+_{\lambda\mu i_1\sigma} = \frac{1}{2}\sum_{qq'}\{\psi^{\lambda\mu i_1}_{qq'}A^+(qq';\mu\sigma) - \phi^{\lambda\mu i_1}_{qq'}A(qq';\mu{-}\sigma)\}. \tag{2}$$

If we take into account electric and magnetic interactions, we write the phonon operator [6] in the form

$$Q^+_{\lambda\mu i_1\sigma} = \frac{1}{2\sqrt{2}}\sum_{qq'}\{\psi^{\lambda\mu i_1}_{qq'}(1{+}i\sigma)A^+(qq';\mu\sigma){-}\phi^{\lambda\mu i_1}_{qq'}(1{-}i\sigma)A(qq';\mu{-}\sigma)\}. \tag{3}$$

The coefficients of the electric part are real; and of the magnetic part, imaginary. Here $i_1 = 1, 2, 3\ldots$ is the root number of the RPA secular equation; $A^+(qq';\mu\sigma)$ and $A(qq';\mu\sigma)$ are, respectively, pair of creation and annihilation quasiparticle operators. The quantum numbers of the single-particle states are denoted by $q\sigma$, where $\sigma = \pm 1$; q equals K^π and asymptotic quantum numbers $Nn_z\Lambda\uparrow$ at $K = \Lambda + 1/2$ and $Nn_z\Lambda\downarrow$ at $K = \Lambda - 1/2$. The RPA one-phonon state is described by the wave function

$$Q^+_{\lambda\mu i\sigma}\Psi_0, \tag{4}$$

where Ψ_0 is the ground state wave function of a doubly even nucleus which is determined as a phonon vacuum. The normalization condition of the wave function (4) has the form

$$\frac{1+\delta_{\mu 0}}{2}\sum_{qq'}[(\psi_{qq'}^{\lambda\mu i_1})^2-(\phi_{qq'}^{\lambda\mu i_1})^2]=1. \tag{5}$$

After some transformation, the QPNM Hamiltonian becomes

$$H_{\rm QPNM}=\sum_{q\sigma}\epsilon_q\alpha_{q\sigma}^{+}\alpha_{q\sigma}+H_v+H_{vq}, \tag{6}$$

where the first two terms describe quasiparticles and phonons, and H_{vq} describes the quasiparticle–phonon interaction.

The one-phonon states form the basis of the QPNM. We, therefore, pay much attention to the solution of the RPA equations. At the next stage, the interaction of quasiparticles with phonons is taken into account. The wave function of the excited state is represented as a series with respect to the number of phonon operators. The approximation consists in the truncation of this series.

The one-phonon states with $K^\pi=0^+$ (denoted by $(\lambda\mu)_i=(20)_i$) are calculated in the RPA with monopole and quadrupole pairing and monopole and ph and pp isoscalar and isovector quadrupole interactions. The relevant RPA equation is given in [6, 7]. The one-phonon states with $K^\pi=1^+$ (denoted by $(21)_i$) are calculated with ph and pp isoscalar and isovector quadrupole and spin–spin interactions. The RPA equations for the $K^\pi=1^+$ one-phonon states are given in [8, 20]. The one-phonon states with $K^\pi=0^-$ and 1^- are calculated in the RPA with the ph and pp isoscalar and isovector octupole and ph isovector dipole interactions. The relevant RPA equations are given in [7, 11]. Other phonons ($\lambda\mu$ = 22, 32, 33, 43, 44, 54, 55, etc.) are calculated with the ph and pp isoscalar and multipole isovector interactions.

To describe nonrotational states in the QPNM, we used a wave function consisting of a sum of one- and two-phonon terms

$$\Psi_n(K_0^{\pi_0}\sigma_0)=\{\sum_{i_0}R_{i_0}^nQ_{g_0}^{+}+\sum_{\substack{g_1g_2\\ \sigma_1\sigma_2}}\frac{(1+\delta_{g_1g_2})^{1/2}}{2[1+\delta_{\mu_0 0}(1-\delta_{\mu_1 0})]^{1/2}}$$
$$\times\delta_{\sigma_1\mu_1+\sigma_2\mu_2,\sigma_0\mu_0}P_{g_1g_2}^nQ_{g_1\sigma_1}^{+}Q_{g_2\sigma_2}^{+}\}\Psi_0. \tag{7}$$

Here $g_0=\lambda_0\mu_0 i_0$, $\mu_0=K_0$, $n=1,2,3\ldots$ is the number of the K_0^π state.

3. DIPOLE STRENGTH DISTRIBUTION IN 0 – 4 MeV ENERGY REGION

3.1. Numerical Procedure. The calculations are made with the Woods–Saxon potential with quadrupole β_2 and hexadecapole β_4 and $\gamma=0$ equilibrium deformations. The single-particle spectrum is taken from the bottom of the potential well up to $+5$ or $+15$ MeV. The parameters of the Woods–Saxon potential were fixed in 1968. $M1$- and $E1$-transition rates from the ground to excited up to 4 MeV states were calculated with the wave functions (7).

The isoscalar constants $\kappa_0^{\lambda\mu}$ of ph interactions are fixed so as to reproduce experimental energies of the first $K^\pi_{n=1}$ nonrotational states. The calculations were made with the isovector constant $\kappa_1^{\lambda\mu} = -1.5\kappa_0^{\lambda\mu}$ for ph interactions and the constant $G^{\lambda\mu} = 0.8\kappa_0^{\lambda\mu}$ for pp interactions. The monopole pairing constants were fixed by pairing energies at $G^{20} = 0.8\kappa_0^{20}$. The radial dependence of the multipole interactions has the form $dV(r)/dr$, where $V(r)$ is the central part of the Woods–Saxon potential. The phonon basis consists of ten ($i_0 = 1, 2, \ldots, 10$) phonons of each multipolarity: $\lambda\mu = 20, 22, 32, 33, 43, 44, 54, 55$, and 65. We used twenty phonons with $\lambda\mu = 21, 30, 31$. The energies of the two-quasiparticle poles were calculated by taking into account the blocking effect and the Gallagher–Moszkowski correction [21]. After the construction of the phonon basis, no free parameters were therefore left. The calculations of nonrotational states in even–even and odd-mass nuclei were performed with the same basis.

3.2. 1^+ **States.** The one-phonon states with $K^\pi = 1^+$ are calculated in the RPA with isoscalar κ_0^{21} and isovector κ_1^{21} ph and pp G^{21} quadrupole–quadrupole and isoscalar κ_0^{011} and isovector κ_1^{011} spin–spin interactions. In both RPA and QPNM the $M1$ strengths were computed by using a bare orbital gyromagnetic factor and an effective spin factor $g_s^{\rm eff} = 0.7 g_s^{\rm free}$.

The spurious state is approximately excluded by choosing the constant $\kappa_0^{21} > (\kappa_0^{21})_{\rm cr}$. The first root of the RPA secular equation equals zero at $(\kappa_0^{21})_{\rm cr}$. The overlap between the one-phonon $Q^+_{21i} >$ and the spurious $< j_-$ states is given by

$$N^i_{\rm sp} = \frac{1}{< j_- j_+ >} < j_- Q^+_{21i} >< Q_{21i} j_+ > . \tag{8}$$

The sum $\sum_i N^i_{\rm sp}$ over the first four states in ^{164}Dy is equal to 0.48 at $\kappa_0^{21} = 0.010$ fm^{2}MeV^{-1} and to 0.008 at $(\kappa_0^{21})_{\rm cr} = 0.01435$ fm^{2}MeV^{-1}. The sums $\sum_i N^i_{\rm sp}$ over the first twenty states up to 4 MeV and over all levels up to 30 MeV in ^{164}Dy are equal to 0.023 and 0.048, respectively. The total overlap $\sum_i N^i_{\rm sp}$ for all levels below 30 MeV in ^{168}Er and ^{238}U is $\sum_i N^i_{\rm sp} = 0.046$ and 0.11, respectively. For any state with $K^\pi = 1^+$ the $N^i_{\rm sp}$ value is smaller than 0.005.

We state that it is not necessary to exclude the spurious state rigorously if a nuclear many-body problem is solved approximately. We performed calculations in the RPA to study the influence of different spurious admixtures on the $M1$ transition rates in ^{166}Er, ^{178}Hf, and ^{238}U. The results of calculations are given in Table 1. The first root of the RPA secular equation in ^{238}U equals zero at $(\kappa_0^{21})_{\rm cr} = 0.0130$ fm^{2}MeV^{-1}. The summed $B(M1)\uparrow$ values of the first twenty states equal 7.0 ± 0.1 μ_N^2 for $\kappa_0^{21} = 0.0130$, 0.0134, 0.0154, 0.0160, and 0.0170 fm^{2}MeV^{-1}. The increase in the summed overlap from 0.018 to 0.063 and in the largest overlap of the single 1^+ state from 0.005 to 0.016 weakly affects the $M1$ strength. The summed overlap $\sum_i N^i_{\rm sp}$ in ^{166}Er and ^{178}Hf decreases with increasing constant κ_0^{21} and strongly increases at $\kappa_0^{21} > 0.018$ fm^{2}MeV^{-1}. An approximate exclusion of the spurious state is reasonably good. The constant κ_0^{21} was fixed differently comparing with other constants $\kappa_0^{\lambda\mu}$. We used the constant κ_0^{21} a little larger than $(\kappa_0^{21})_{\rm cr}$ for better description of the first $K_n^\pi = 1_1^+$ state. As is shown in Table 1, the summed $B(M1)\uparrow$ values weakly depend on κ_0^{21}. The constant $(\kappa_0^{21})_{\rm cr}$ equals 0.013–0.015 fm^{2}MeV^{-1} in ^{156,158,160}Gd, ^{160,162,164}Dy, ^{166,168}Er, ^{178}Hf, ^{238}U, and ^{240}Pu. The present calculations are performed with the constant κ_0^{21} equal to 0.015 fm^{2}MeV^{-1}.

Table 1. Summed overlaps with the spurious and scissors states and $M1$ and $E2$ strengths calculated for different constants κ_0^{21} in the energy range 2–4 MeV in ^{166}Er and ^{178}Hf and in 1–3 MeV in ^{238}U

Nucleus	κ_0^{21} fm^{2}MeV^{-1}	$\sum_i N^i_{\rm sp}$	$\sum_i Sc^i$	$\sum_i B(M1)^i\uparrow$ μ_N^2	$\sum_i B(E2)^i\uparrow$ s.p.u.
^{166}Er	0.0143	0.032	0.41	5.11	2.27
	0.0154	0.017	0.42	5.13	1.91
	0.0164	0.012	0.43	5.23	1.68
^{178}Hf	0.0133	0.045	0.31	4.05	2.67
	0.0152	0.013	0.32	3.94	1.98
	0.0164	0.016	0.34	4.04	2.02
^{238}U	0.0130	0.018	0.49	7.10	1.71
	0.0154	0.028	0.52	7.02	1.43
	0.0170	0.063	0.55	6.98	1.41

We used the constant $G^{\lambda\mu}$ of pp interactions equal to $0.8\kappa_0^{\lambda\mu}$ for all $\lambda\mu$ including $\lambda\mu = 21$. As is shown in [22] and in the present calculations, the summed $\sum B(M1)\uparrow$ in the energy range 1–4 MeV increased by a factor of 1.2–1.4 at $G^{21} = \kappa_0^{21}$ compared with $G^{21} = 0.8\kappa_0^{21}$. This sum decreased by a factor of 0.8–0.9 at $G^{21} = 0$ compared with $G^{21} = 0.8\kappa_0^{21}$. The summed $\sum B(M1)\uparrow$ weakly depends on κ_1^{21}. This sum does not practically change at $\kappa_1^{21} = -\kappa_0^{21}$ compared with $\kappa_1^{21} = -1.5\kappa_0^{21}$, it increases by a factor of 1.5 at $\kappa_1^{21} = 0$. We used $\kappa_1^{21} = -1.5\kappa_0^{21}$ in the rare-earth and $\kappa_1^{21} = -1.2\kappa_0^{21}$ in the actinide regions. A critical analysis of the choice of the constant κ_1^{21} in [23] leads to values which are reasonably close to our value. We correctly described giant isoscalar and isovector quadrupole resonance with these constants.

We used the isoscalar κ_0^{011} and isovector κ_1^{011} constants of the ph spin–spin interaction equal to -0.0024 and -0.024 fm^{2}MeV^{-1}. The $M1$ strength in the low energy region depends weakly on κ_1^{011} and κ_0^{011}. The summed $\sum B(M1)\uparrow$ up to 3 MeV in ^{240}Pu increases by a factor of 1.24 at $\kappa_1^{011} = -0.0024$ and decreases by a factor of 1.24 at $\kappa_1^{011} = -0.24$ compared with $\kappa_1^{011} = -0.024$ fm^{2}MeV^{-1}. The summed spin $M1$ strength in the range 1–15 MeV in ^{154}Sm increases by a factor of 1.25 at $\kappa_1^{011} = -0.012$ compared with $\kappa_1^{011} = -0.048$ fm^{2}MeV^{-1}. The calculated spin $M1$ strength in ^{154}Sm summed up to 12 MeV at $\kappa_1^{011} = -0.024$ fm^{2}MeV^{-1}, equal to 11.5 μ_N^2, is close to the calculated value of 11.4 μ_N^2 in [24]. The calculated spin $M1$ strength in ^{154}Sm summed in the energy range 5–10 MeV at $\kappa_1^{011} = -0.024$ fm^{2}MeV^{-1}, equal to 9.5 μ_N^2, does not contradict the experimental $M1$ strength $\sum B_\sigma(M1) = 11 \pm 2\ \mu_N^2$ [15].

3.3. $K^\pi = 0^-$ and 1^- States. The origin of $E1$ strength in the low-energy region in deformed nuclei has been investigated in [25]. It is known that there are no one-phonon 1^- states below the particle threshold in spherical nuclei. Quadrupole deformation is responsible for the splitting of subshells of a spherical basis into twice-degenerate single-particle states. Due to this splitting, part of the $E1$ strength is shifted to low-lying states. An octupole isoscalar interaction between quasiparticles leads to the formation of collective octupole states. Due to the octupole interaction, the summed $E1$ strength for the transition to $K^\pi = 0^-$ and 1^- states in the (0–4) MeV energy region increases by two orders of magnitude. An isovector dipole ph interaction shifts the largest part of $E1$ strength from the low-lying states to the region of the isovector GDR.

The one-phonon states with $K^\pi = 0^-$ and 1^- are calculated in the RPA with ph and pp isoscalar and isovector octupole and ph isovector dipole interactions. The isovector constant of the ph dipole interaction is $\kappa_1^{1\mu} = -1.5\kappa_0^{3\mu}$ for the rare-earth and $\kappa_1^{1\mu} = -1.2\kappa_0^{3\mu}$ for the actinide nuclei. The GDR was correctly described with these constants $\kappa_1^{1\mu}$.

In the low-energy region, the isovector ph electric dipole interaction reduces the $E1$ strength by more than an order of magnitude [11]. Such a reduction, however, is not sufficient, since the calculated $B(E1)$ values for the excitation of the $K^\pi = 0^-$ states remain 3–10 times the experimental ones. For a further quenching needs an effective charge is to be used. Physically, this quantity should account for the coupling of the low with the high energy configurations excluded from the model space. We used the following renormalized effective charge

$$e_{\text{eff}}^{(1)} = -\frac{e}{2}(\tau_z - \frac{N-Z}{A})(1+\chi), \tag{9}$$

where the factor χ is a fitting parameter introduced to quench the too large $E1$ transition probabilities at $\chi = 0$. In many papers, for example in Ref. 26, the value $(1+\chi) = 0.3$ was chosen. We computed the $E1$ reduced transition probabilities in ^{168}Er within the QPNM and fixed χ by an overall fit of the experimental summed strength in the energy range 1.7–4.0 MeV [27] obtaining $(1+\chi) = \sqrt{0.2}$. This value was adopted to study within the QPNM the $E1$ strength distribution in doubly even deformed nuclei over an energy interval up to 4 MeV [9–11]. The computed $B(E1)$ values where quenched by a factor 5 in qualitative agreement with the experimental data. In this low-energy region, the total strength of the $E1$ transitions to the $K^\pi = 0^-$ states in the Gd, Dy, Er and Yb isotopes resulted to be 2–4 times larger than the strength of the transitions to the $K^\pi = 1^-$ states. An exception is represented by the ^{178}Hf nucleus where the $E1$ $\Delta K = 0$ summed strength is partly suppressed.

3.4. Numerical Results. The $K^\pi = 1^+$ states below 2 MeV have been observed in one-nucleon transfer reactions and in β decays in a number of even–even deformed nuclei. Most of the properties of the collective scissors mode have been established in (e, e') and (γ, γ') experiments. Microscopic calculations of the $K^\pi = 1^+$ states and $B(M1)\uparrow$ values have been carried out so far in the RPA. We calculated in the RPA and QPNM the energies and wave functions of the $K^\pi = 1^+$ states and $B(M1)\uparrow$ values in ^{156,158,160}Gd, ^{160,162,164}Dy, and ^{238}U. These results were published in [8,9,20]. Our results of the RPA calculations of the $M1$ strength distribution do not practically differ compared to the calculations [24, 28, 29].

The results of calculations of the energies, wave functions and $B(M1)\uparrow$ and $B(E1)\uparrow$ values in ^{166,168}Er, ^{172,174}Yb, ^{178}Hf, and ^{238}U are given in the form of Tables or Figures. The experimental data as well as the results of our calculations are presented in Tables 2, 3, 4, 5, 6, 10. The calculated structure is given as a contribution of the one-phonon $(\lambda\mu)_i$ and two-phonon $\{(\lambda_1\mu_1)_{i_1}, (\lambda_2\mu_2)_{i_2}\}$ components to the normalization of the wave function (7). Then, we list the largest two-quasineutron $\nu\nu$ and two-quasiproton $\pi\pi$ components of the wave function (4) of the one-phonon state $(\lambda\mu)_i$. The $B(E\lambda)\uparrow \equiv B(E\lambda; 0^+0_{\rm g.s.} \to I^\pi K_n)$ with $I = \lambda$ for $\lambda \geq 2$ is given in the single-particle units

$$B(E\lambda)\uparrow_{\rm s.p.u.} = \frac{2\lambda+1}{4\pi}\left(\frac{3}{\lambda+3}\right)^2 (0.12A^{1/3})^{2\lambda} \quad e^2(10\ {\rm fm})^{2\lambda}. \qquad (10)$$

3.5. Scissors Mode. The wave function of the scissors state has been defined [30] as

$$\Psi_{sc} = (< j_- j_+ >< j_- j_+ >_\nu < j_- j_+ >_\pi)^{-1/2} [I_+(\nu) < j_- j_+ >_\pi$$
$$- I_+(\pi) < j_- j_+ >_\nu] \Psi_0 \qquad (11)$$

with the normalization condition

$$(\Psi^*_{sc}\Psi_{sc}) = 1.$$

Here

$$I_\pm(\tau) = \sum_{i_0} I_\pm^{21 i_0}(\tau) \frac{1 \mp i}{\sqrt{2}} (Q^+_{21 i_0 \pm} - Q_{21 i_0 \mp}),$$

$$I_{\pm}^{21i_0}(\tau) = \sum_{q_1>q_2}^{\tau} < q_1|j_{\pm}|q_2 > u_{q_1q_2}^{(-)}\psi_{q_1q_2}^{21i_0}.$$

The wave function Ψ_{sc} is orthogonal to the spurious state $j_+\Psi_0$. The overlap is calculated in the RPA so as to enforce the following normalization condition

$$\sum_i |(\Psi_{sc}^* Q_{21i\sigma_0}^+ \Psi_0)|^2 = 1,$$

where the sum extends to all RPA states. The overlap of the wave function (7) with the scissors state has the following form:

$$Sc^n = \frac{1}{< j_-j_+ >< j_-j_+ >_\nu < j_-j_+ >_\pi} \sum_{i_0 i_0'} R_{i_0}^n R_{i_0'}^n$$
$$\times [< j_-j_+ >_\pi I_+^{21i_0}(\nu) - < j_-j_+ >_\nu I_+^{21i_0}(\pi)]$$
$$\times [< j_-j_+ >_\pi I_+^{21i_0'}(\nu) - < j_-j_+ >_\nu I_+^{21i_0'}(\pi)]. \quad (12)$$

According to our calculations, the scissors mode fragments over both the low- and high-energy $M1$ excitations. The overlap of scissors with low-lying states up to 4 MeV is about 50%. The other half goes to the high-energy states in the range 20–24 MeV. This is consistent with the schematic predictions of the existence of two scissors modes, one at low and the other at high energies [31]. The scissors state is strongly fragmented in the low-energy region. According to [32] and our calculations, for any 1_n^+ state the Sc^n value is smaller than 0.2. The results on the overlap with the scissors state are similar in RPA and QPNM.

The reduced probability for $M1$ transition from the ground state $0_{\rm g.s.}^+$ to the 1_{sc}^+ scissors state is

$$B_{sc}(M1; 0_{\rm g.s.}^+ \to 1_{sc}^+) = 2\mu_N^2 |(\Psi_{sc}^* \Gamma(M1)\Psi_0)|^2$$
$$= 2\mu_N^2 |\sum_i \mathcal{A}(M1; 0_{\rm g.s.}^+ \to 1_i^+)|^2, \quad (13)$$

where $\Gamma(M1)$ is the magnetic dipole operator, $\mathcal{A}(M1; 0_{\rm g.s.}^+ \to 1_i^+)$ is the amplitude for $M1$ transition to a relevant one-phonon component i of the wave function (11). The sum over i extends to all RPA states. A contribution of the scissors components of the one-phonon state i to the $B(M1)_i$ value equals 10^{-5}–10^{-1}. The ratio

$$\frac{\sum_i B_{sc}(M1\uparrow)_i}{\sum_i B(M1\uparrow)_i} = 0.05$$

for the sum over all the RPA states below 4 MeV for each scissors component $B_{sc}(M1)_i$. According to calculation with Eq. (13), the ratio

$$\frac{B_{sc}(M1; 0_{\rm g.s.}^+ \to 1_{sc}^+)}{\sum_i B(M1\uparrow)_i} = 0.3 - 0.4.$$

It means that the scissors contribution to the total $M1$ strength in the energy range 1–4 MeV is large due to the coherence effect.

The scissors mode is mostly responsible for enhanced total $M1$ strength in the low-energy region. The contribution of the scissors state to the total $M1$ strength in the energy range up to 30 MeV in ^{168}Er equals 60%. The large contribution to the total $M1$ strength in the energy range 2–30 MeV is due to the coherence sum in Eq. (13). Nevertheless, its contribution to the wave functions of each 1^+ states is small. The wave functions of $K^\pi = 1^+$ states are mostly determined by other components which may be observed, for example, by one-nucleon-transfer reactions.

3.6. $K^\pi = 1^+$ States and $M1$ Strength Distribution. The fragmentation of the one-phonon $K^\pi = 1^+$ states in ^{156,158,160}Gd and ^{160,162,164}Dy has been studied in the QPNM in [8, 20]. In each of these nuclei there is a strong peak of an order of 1–1.5 μ_N^2. The fragmentation is appreciable only above 3 MeV.

In our investigation of the fragmentation of one-phonon states we paid special attention to ^{168}Er because the parities of the excited states have been determined model independently by measuring the linear polarization of the scattered photons. Experimental energies of the 1^+ states and $B(M1)\uparrow$ values [27] are compared with the calculated ones in Table 2. The $B(E2)\uparrow$ values characterize the collectivity of each state. The structure of each $K^\pi = 1^+$ state is presented. The 1^+ levels below 2.3 MeV in ^{168}Er have not been observed experimentally. It is impossible to compare one to one the experimental and computed levels. The experimental and computed $M1$ strength distributions in ^{166}Er are given in Fig. 1. In general, the observed $M1$ strength in ^{168}Er and ^{166}Er is stronger fragmented than in the Gd and Dy isotopes. The fragmentation of one-phonon states due to the coupling with two-phonon configurations is very important above 3 MeV in both nuclei. The observed $M1$ strength in ^{166,168}Er is stronger fragmented below 3 MeV than the calculated ones.

Table 2. Energies, $M1$ and $E2$ strengths and structure of the QPNM $K^\pi = 1^+$ states in ^{168}Er

n	Experiment [27]		Calculation in the QPNM			
	E_n MeV	$B(M1)\uparrow$ μ_N^2	E_n MeV	$B(M1)\uparrow$ μ_N^2	$B(E2)\uparrow$ s.p.u.	Structure, %
1			2.10	0.05	0.06	$(21)_1$ 82; $(21)_3$ 7 $\{(31)_1,(32)_1\}$ 5 $(21)_1$: $\nu\nu633\uparrow$-$642\uparrow$ 80 $\nu\nu624\uparrow$-$633\uparrow$ 13 $\pi\pi514\uparrow$-$523\uparrow$ 3

Table 2. (cont.)

	Experiment [27]		Calculation in the QPNM			
n	E_n MeV	$B(M1)\uparrow$ μ_N^2	E_n MeV	$B(M1)\uparrow$ μ_N^2	$B(E2)\uparrow$ s.p.u.	Structure, %
2			2.29	0.04	0.02	$(21)_2$ 93 $\{(32)_1,(33)_3\}$ 2 $(21)_2$: $\pi\pi411\uparrow$-$411\downarrow$ 98
3	2.494	0.162 ± 0.018	2.33	1.05	0.32	$(21)_1$ 12; $(21)_2$ 3 $(21)_3$ 65; $(21)_5$ 5 $\{(31)_1,(32)_1\}$ 6 $\{(33)_2,(54)_1\}$ 5 $(21)_3$: $\nu\nu624\uparrow$-$633\uparrow$ 62 $\pi\pi514\uparrow$-$523\uparrow$ 24 $\nu\nu512\uparrow$-$521\uparrow$ 7 $\nu\nu633\uparrow$-$642\uparrow$ 3
4	2.643	(0.063 ± 0.013)	2.60	0.02	$2 \cdot 10^{-5}$	$(21)_4$ 88 $\{(32)_1,(33)_1\}$ 5 $(21)_4$ $\nu\nu521\uparrow$-$521\downarrow$ 91 $\nu\nu512\uparrow$-$521\uparrow$ 6
5	2.676	0.171 ± 0.18	2.66	1.05	0.01	$(21)_3$ 9; $(21)_5$ 81 $\{(31)_1,(32)_1\}$ 3 $(21)_5$: $\pi\pi514\uparrow$-$523\uparrow$ 44 $\nu\nu512\uparrow$-$521\uparrow$ 39 $\nu\nu521\uparrow$-$521\downarrow$ 6
6	2.694	(0.025 ± 0.005)	2.77	0.02	$1 \cdot 10^{-3}$	$(21)_6$ 97 $(21)_6$: $\nu\nu514\downarrow$-$512\uparrow$ 98
7	2.728	(0.262 ± 0.029)	2.85	0.18	0.29	$(21)_7$ 81 $\{(22)_1,(43)_1\}$ 6 $(21)_7$: $\nu\nu514\downarrow$-$523\downarrow$ 33 $\nu\nu512\uparrow$-$521\uparrow$ 33 $\pi\pi404\downarrow$-$413\downarrow$ 10 $\pi\pi523\uparrow$-$532\uparrow$ 7 $\pi\pi514\uparrow$-$523\uparrow$ 5

Table 2. (cont.)

	Experiment [27]		Calculation in the QPNM			
n	E_n MeV	$B(M1)\uparrow$ μ_N^2	E_n MeV	$B(M1)\uparrow$ μ_N^2	$B(E2)\uparrow$ s.p.u.	Structure, %
9	2.792	0.179 ± 0.019	3.05	0.24	0.01	$(21)_{10}$ 68 $\{(31)_1,(32)_1\}$ 14 $\{(33)_2,(54)_1\}$ 4
10	2.798	0.208 ± 0.021	3.11	0.12	0.08	$(21)_7$ 4; $(21)_9$ 65 $(21)_{12}$ 11 $\{(22)_1,(43)_1\}$ 9
11	3.048	(0.105 ± 0.014)	3.16	0.58	$1 \cdot 10^{-3}$	$(21)_7$ 6; $(21)_9$ 33 $(21)_{12}$ 25; $(21)_{13}$ 6 $\{(22)_1,(43)_1\}$ 14 $\{(32)_1,(33)_1\}$ 5 $\{(33)_2,(54)_1\}$ 5
12	3.357	(0.348 ± 0.041)	3.22	0.11	$3 \cdot 10^{-3}$	$(21)_{10}$ 11; $(21)_{12}$ 3 $(21)_{13}$ 4; $(21)_{14}$ 4 $\{(33)_2,(54)_1\}$ 51 $\{(31)_1,(32)_1\}$ 13 $\{(22)_1,(43)_1\}$ 8
13	3.390	0.753 ± 0.086	3.29	0.22	0.03	$(21)_4$ 3; $(21)_5$ 3 $(21)_{13}$ 4; $(21)_{14}$ 7 $\{(32)_1,(33)_1\}$ 69 $\{(33)_2,(54)_1\}$ 3 $\{(22)_1,(43)_1\}$ 3 $\{(21)_1,(22)_1\}$ 2
14	3.409	(0.234 ± 0.029)	3.34	0.08	$1 \cdot 10^{-4}$	$(21)_{12}$ 10; $(21)_{13}$ 18 $\{(21)_1,(22)_1\}$ 65 $\{(32)_1,(33)_1\}$ 4
17	3.457	0.319 ± 0.039	3.41	0.02	0.02	$\{(33)_1,(54)_1\}$ 92
18	3.591	(0.055 ± 0.010)	3.44	0.06	0.02	$(21)_3$ 8; $(21)_5$ 4 $(21)_{10}$ 7 $\{(31)_1,(32)_1\}$ 49 $\{(33)_2,(54)_1\}$ 15
19	3.657	(0.191 ± 0.026)	3.48	0.13	0.16	$(21)_{12}$ 3; $(21)_{14}$ 27 $\{(32)_1,(33)_2\}$ 27 $\{(44)_1,(43)_1\}$ 5 $\{(22)_1,(33)_1\}$ 10 $\{(33)_1,(54)_1\}$ 5

Table 2. (cont.)

n	Experiment [27] E_n MeV	$B(M1)\uparrow$ μ_N^2	Calculation in the QPNM E_n MeV	$B(M1)\uparrow$ μ_N^2	$B(E2)\uparrow$ s.p.u.	Structure, %
26	3.776	(0.054 ± 0.010)	3.74	0.05	$4 \cdot 10^{-5}$	$(21)_{12}$ 9; $(21)_{13}$ 8
						$(21)_{14}$ 4
						$\{(22)_1,(43)_1\}$ 31
						$\{(33)_3,(54)_1\}$ 22
42	3.806	0.204 ± 0.033	3.94	0.04	0.01	$(21)_{15}$ 7
						$\{(30)_1,(31)_2\}$ 81

The experimental and calculated $M1$ strength distribution in ^{172}Yb is given in Fig. 2. The experimental and calculated energies and $B(M1)\uparrow$ values in ^{174}Yb are presented in Table 3. The first $K_n^\pi = 1_1^+$ state with energy 1.624 MeV in ^{174}Yb is, practically, pure two-quasineutron state. This state was observed in the (d,p) reaction [34]. This two-quasineutron $\nu\nu514\downarrow-512\uparrow$ state was not observed in ^{172}Yb. The second $K_n^\pi = 1_2^+$ 2.01 MeV state in ^{172}Yb was observed in the (d,t) reaction. Most levels with $K^\pi = 1^+$ in ^{172}Yb and ^{174}Yb were observed in the (γ,γ') experiments [33] with uncertain parity assignments. The parity of the levels with energy 3.349 and 3.562 MeV in ^{174}Yb are known from the (e,e') experiments [35]. According to our calculation, the two-quasiproton state $\pi\pi404\downarrow-413\downarrow$ is fragmented in the energy range 3.5–3.9 MeV in ^{174}Yb. Therefore, this configuration has not been observed in the (t,α) reaction [36].

A comparison of the observed $M1$ strength distribution in ^{178}Hf [37] with the result of the present calculations within the RPA and QPNM is demonstrated in Fig. 3. The strong fragmentation of the $M1$ strength in the energy range 2.4–4.0 MeV is well described in the QPNM. According to the RPA calculation, there is a strong peak of 1.05 μ_N^2 at 3.64 MeV. This one-phonon state is strongly fragmented in the energy range 3.2–4.0 MeV. The coupling between one- and two-phonon states is responsible for strong fragmentation of the $M1$ strength in ^{178}Hf.

The experimental [38, 39] and calculated energies and $B(M1)\uparrow$ values in ^{238}U are presented in Table 4. According to the calculation, the $K^\pi = 1^+$ levels at 1.68 and 1.86 MeV have $B(M1)\uparrow$ equal to 0.61 and 0.62 μ_N^2, respectively. In the case of positive parity of $K = 1$ levels at 1.782 and 1.846 MeV the $B(M1)\uparrow$ strength is (0.43±0.05) and (0.41±0.06) μ_N^2 [39].

There are strong dipole $K^\pi = 0^-$ and 1^- excitations in ^{238}U (see below). To summarize, we have described the strong dipole excitations around 1.8 MeV in ^{238}U which have been found in [39].

Twenty-two levels in ^{238}U have been observed in [40] with 18 MeV ^{4}He ions. Eight 2^+ states between 0.966 and 1.782 MeV and three 3^- states are populated

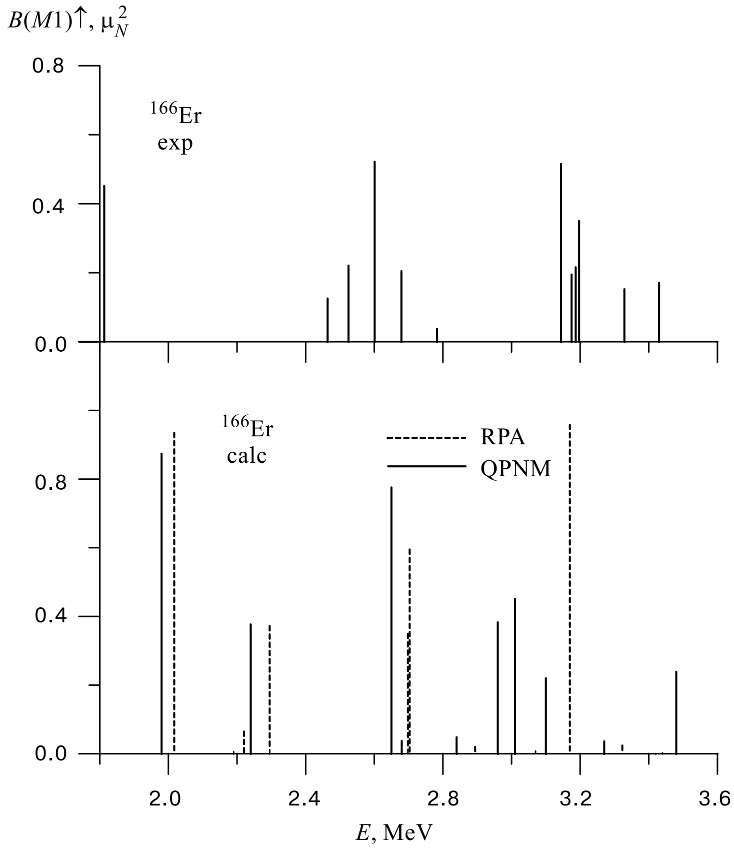

Fig. 1. Experimental, QPNM and RPA $M1$ strength distribution in ^{166}Er. Full and dashed lines refer respectively to QPNM and RPA

by direct $E2$ and $E3$ transitions, respectively. This is an unusually large number of 2^+ states in this low excitation region. Three of the 2^+ states with energies 1.530, 1.414, and 1.224 MeV have decay branches to the one-phonon states with $B(E2)$ values between 27 and 56 W.u. which are an order of magnitude larger than the $B(E2)$ values between one-phonon and ground states. These $B(E2)$ values are in disagreement with the calculation within the QPNM [41]. These decay branches are much larger than the corresponding $B(E2)$ ratios in the harmonic limit. The results obtained in [40] are in conflict with any microscopic description of nuclear vibrational states. It is challenge to the theory of atomic nuclei. Therefore, it is tempting to reconsider the $E2$ assignment and explore the possibility that the observed transitions have a different nature. To this purpose we have computed the $E2$ and $M1$ strengths.

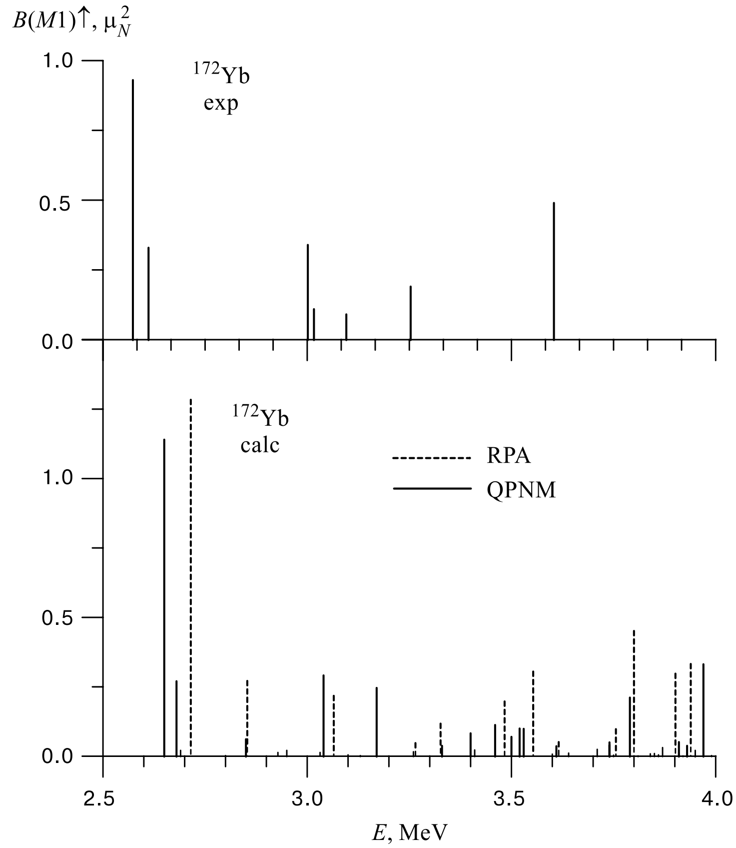

Fig. 2. Experimental, QPNM and RPA $M1$ strength distribution in ^{172}Yb. See Fig. 1 for explanatory details

Table 3. Energies, $M1$ and $E2$ strengths and structure of the QPNM $K^\pi = 1^+$ states in ^{174}Yb

n	Experiment [33]		Calculation in the QPNM			
	E_n MeV	$B(M1)\uparrow$ μ_N^2	E_n MeV	$B(M1)\uparrow$ μ_N^2	$B(E2)\uparrow$ s.p.u.	Structure, %
1	1.624		1.60	$1.3 \cdot 10^{-3}$	$3 \cdot 10^{-4}$	$(21)_1$ 99 $(21)_1$: $\nu\nu$514↓-512↑ 99
2	2.037 2.068	0.15 ± 0.11 0.20 ± 0.12	2.10	0.86	0.87	$(21)_2$ 99 $(21)_2$: $\nu\nu$624↑-633↑ 72

Table 3. (cont.)

n	Experiment [33]		Calculation in the QPNM			
	E_n MeV	$B(M1)\uparrow$ μ_N^2	E_n MeV	$B(M1)\uparrow$ μ_N^2	$B(E2)\uparrow$ s.p.u.	Structure, %
						$\pi\pi514\uparrow$-$523\uparrow$ 13
3	2.338	0.28 ± 0.10	2.65	0.92	0.02	$(21)_3$ 85; $(21)_5$ 1
	2.500	0.35 ± 0.11				$(21)_6$ 2
						$\{(22)_1,(43)_1\}$ 2
						$\{(31)_2,(32)_1\}$ 3
						$\{(32)_1,(33)_1\}$ 1
						$\{(54)_1,(55)_1\}$ 2
						$(21)_3$:
						$\pi\pi514\uparrow$-$523\uparrow$ 45
						$\nu\nu633\uparrow$-$642\uparrow$ 30
						$\nu\nu512\uparrow$-$521\uparrow$ 15
						$\nu\nu514\downarrow$-$523\downarrow$ 5
5	2.581	(0.21 ± 0.08)	2.69	0.11	0.06	$(21)_5$ 55; $(21)_6$ 18
						$(21)_8$ 2
						$\{(32)_1,(33)_1\}$ 12
						$\{(31)_2,(32)_1\}$ 3
						$(21)_5$:
						$\nu\nu615\uparrow$-$624\uparrow$ 38
						$\nu\nu633\uparrow$-$642\uparrow$ 25
						$\pi\pi514\uparrow$-$523\uparrow$ 16
						$\nu\nu510\uparrow$+$521\downarrow$ 9
						$\nu\nu512\uparrow$-$521\uparrow$ 6
11	2.920	(0.44 ± 0.11)	3.06	0.25	0.03	$(21)_8$ 5; $(21)_9$ 8
						$(21)_{10}$ 63; $(21)_{11}$ 6
						$\{(21)_1,(22)_1\}$ 1
						$\{(21)_1,(43)_1\}$ 2
						$\{(31)_1,(32)_1\}$ 9
						$(21)_{10}$:
						$\nu\nu512\uparrow$-$512\downarrow$ 66
						$\pi\pi411\uparrow$-$411\downarrow$ 24
						$\nu\nu514\downarrow$-$523\downarrow$ 5
14	3.122	(0.10 ± 0.06)	3.21	0.30	0.16	$(21)_{11}$ 28; $(21)_{12}$ 43
	3.145	(0.13 ± 0.06)				$(21)_{13}$ 3; $(21)_{15}$ 5
						$\{(22)_1,(43)_1\}$ 2
						$\{(22)_1,(43)_2\}$ 7
						$\{(31)_2,(32)_1\}$ 3

Table 3. (cont.)

n	Experiment [33] E_n MeV	$B(M1)\uparrow$ μ_N^2	Calculation in the QPNM E_n MeV	$B(M1)\uparrow$ μ_N^2	$B(E2)\uparrow$ s.p.u.	Structure, %
17	3.349	0.33 ± 0.14	3.35	0.56	0.18	$(21)_{11}$ 4; $(21)_{12}$ 22 $(21)_{13}$ 13; $(21)_{15}$ 14 $\{(22)_1,(43)_1\}$ 30 $\{(32)_1,(33)_1\}$ 3
23	3.562	0.41 ± 0.10	3.57	0.25	0.02	$(21)_{12}$ 4; $(21)_{13}$ 30 $(21)_{15}$ 13; $(21)_{16}$ 8 $\{(22)_1,(43)_2\}$ 9 $\{(22)_1,(43)_3\}$ 3 $\{(32)_1,(33)_1\}$ 19 $\{(32)_1,(33)_2\}$ 3
25	3.695	(0.33 ± 0.13)	3.65	0.11	0.03	$(21)_{13}$ 3; $(21)_{15}$ 5 $\{(21)_2,(20)_1\}$ 66 $\{(22)_1,(43)_1\}$ 11 $\{(43)_1,(44)_2\}$ 4
31			3.75	0.22	0.007	$(21)_{15}$ 3; $(21)_{16}$ 3 $\{(54)_1,(55)_1\}$ 82
33			3.84	0.13	0.11	$(21)_{15}$ 5; $(21)_{16}$ 11 $(21)_{17}$ 4 $\{(21)_2,(22)_1\}$ 41 $\{(22)_1,(43)_2\}$ 10
35			3.87	0.11	0.09	$(21)_{15}$ 5; $(21)_{16}$ 9 $(21)_{17}$ 3 $\{(21)_2,(22)_1\}$ 37 $\{(22)_1,(43)_2\}$ 17 $\{(22)_1,(43)_3\}$ 14

The γ-ray transitions between 2^+ states were treated in [40] as $E2$ transitions and were rejected as $M1$ transitions. According to our calculation, there are relatively strong $M1$ transitions between 2^+ states. It is possible to expect that the Coriolis coupling between the 2^+ state at 1.530 MeV and the 2^+ member of a rotational band based on the $K^\pi = 1^+$ state at 1.782 MeV are responsible for a large $B(M1)$ value for the transition from the 2^+ state at 1.530 MeV to the 2^+0_1 state at 0.966 MeV.

The energies, $B(E2)\uparrow$, $B(E2; 2^+ \to 2'^+)$ and $B(M1; 2^+ \to 2'^+)$ values observed in [40] and calculated are presented in Fig. 4. We do not include in Fig. 4 the 2^+ state at 1.530 MeV. According to [40], the B(E2) value for the decay branch into the one-phonon quadrupole state at 0.966 MeV is 56 W.u.

Table 4. Energies, $M1$ and $E2$ strength and structure of the $K^{\pi}{=}1^{+}$ states in ^{238}U

n	Experiment [ref]		Calculation in QPNM			
	E_n MeV	$B(M1)\uparrow$ μ_N^2	E_n MeV	$B(M1)\uparrow^a$ μ_N^2	$B(E2)\uparrow^b$ s.p.u.	Structure, %
1			1.18	0.032	0.02	$(21)_1$ 97 $\{(31)_1,(32)_1\}$ 1 $(21)_1$: $\nu\nu 624\downarrow - 622\uparrow$ 99
2	1.782	0.43 ± 0.05 [39]	1.68	0.61	0.22	$(21)_2$ 76; $(21)_3$ 3 $\{(31)_1,(32)_1\}$ 12 $(21)_2$: $\nu\nu 734\uparrow - 743\uparrow$ 67 $\pi\pi 642\uparrow - 651\uparrow$ 25 $\nu\nu 624\downarrow - 633\downarrow$ 3
3	1.846	0.41 ± 0.06 [39]	1.85	0.62	0.07	$(21)_2$ 4; $(21)_3$ 93 $(21)_3$: $\pi\pi 642\uparrow - 651\uparrow$ 69 $\nu\nu 734\uparrow - 743\uparrow$ 14 $\nu\nu 624\downarrow - 633\downarrow$ 7 $\nu\nu 743\uparrow - 752\uparrow$ 3
4			1.97	0.34	0.07	$(21)_2$ 13; $(21)_5$ 16 $(21)_8$ 15 $\{(31)_1,(32)_1\}$ 48
5			2.07	0.04	0.03	$(21)_4$ 87; $(21)_5$ 2 $\{(22)_1,(43)_2\}$ 2 $(21)_4$: $\nu\nu 624\downarrow - 633\downarrow$ 63 $\nu\nu 613\uparrow - 622\uparrow$ 30 $\pi\pi 642\uparrow - 402\downarrow$ 3
6			2.14	0.01	$6 \cdot 10^{-3}$	$(21)_4$ 3; $(21)_5$ 46 $(21)_6$ 34; $(21)_7$ 4 $\{(31)_1,(32)_1\}$ 4 $(21)_5$: $\nu\nu 743\uparrow - 752\uparrow$ 55 $\nu\nu 613\uparrow - 622\uparrow$ 28 $\nu\nu 624\downarrow - 633\downarrow$ 8
7	2.176 (γ,γ') : 0.93 ± 0.06 (e,e') : 1.25 ± 0.30		2.18	1.60	0.08	$(21)_5$ 24; $(21)_6$ 58 $(21)_8$ 9 $\{(31)_1,(32)_1\}$ 4 $(21)_6$:

Table 4. (cont.)

n	Experiment [ref]		Calculation in QPNM			
	E_n MeV	$B(M1)\uparrow$ μ_N^2	E_n MeV	$B(M1)\uparrow^a$ μ_N^2	$B(E2)\uparrow^b$ s.p.u.	Structure, %
		[38]				$\pi\pi 642\uparrow - 402\downarrow$ 77
						$\nu\nu 743\uparrow - 752\uparrow$ 18
						$\nu\nu 613\uparrow - 622\uparrow$ 4
8	2.209		2.25	0.80	0.20	$(21)_5$ 4; $(21)_7$ 83
		$(\gamma,\gamma') : 0.90 \pm 0.06$				$\{(31)_1, (32)_1\}$ 3
		$(e,e') : 0.88 \pm 0.35$				$(21)_7$:
		[38]				$\pi\pi 521\uparrow - 530\uparrow$ 34
						$\nu\nu 743\uparrow - 752\uparrow$ 18
						$\nu\nu 613\uparrow - 622\uparrow$ 15
						$\nu\nu 622\uparrow - 631\uparrow$ 13
						$\pi\pi 642\uparrow - 402\downarrow$ 7
9	2.245		2.35	0.50	$2 \cdot 10^{-3}$	$(21)_6$ 3; $(21)_7$ 3
						$(21)_9$ 40
		$(\gamma,\gamma') : 0.48 \pm 0.03$				$(21)_{10}$ 19; $(21)_{11}$ 12
		$(e,e') : 0.64 \pm 0.28$				$\{(30)_2, (31)_1\}$ 4
		[38]				$\{(22)_1, (43)_1\}$ 3
						$\{(32)_1, (33)_1\}$ 3
						$(21)_9$:
						$\nu\nu 631\uparrow - 631\downarrow$ 98
10	2.295		2.40	0.19	0.02	$(21)_9$ 35; $(21)_{10}$ 40
		$(\gamma,\gamma') : 0.19 \pm 0.02$				$\{(30)_2, (31)_1\}$ 4
		$(e,e') : 0.23 \pm 0.18$				$\{(32)_1, (33)_1\}$ 5
		[38]				$(21)_{10}$:
						$\pi\pi 523\downarrow - 521\uparrow$ 91
						$\nu\nu 615\downarrow - 624\downarrow$ 4
11			2.41	0.003	0.09	$(21)_8$ 25; $(21)_9$ 19
						$(21)_{10}$ 13
						$\{(31)_1, (32)_1\}$ 10
						$\{(22)_1, (43)_1\}$ 9
						$(21)_8$:
						$\nu\nu 622\uparrow - 631\uparrow$ 65
						$\pi\pi 521\uparrow - 530\uparrow$ 31
12	2.410		2.48	0.19	$6 \cdot 10^{-3}$	$(21)_8$ 20; $(21)_{10}$ 9
						$(21)_{11}$ 37
		$(\gamma,\gamma') : 0.33 \pm 0.03$				$\{(31)_1, (32)_1\}$ 9
		$(e,e') : 0.48 \pm 0.25$				$\{(22)_1, (43)_2\}$ 7
		[38]				$(21)_{11}$:

Table 4. (cont.)

n	Experiment [ref] E_n MeV	$B(M1)\uparrow$ μ_N^2	Calculation in QPNM E_n MeV	$B(M1)\uparrow^a$ μ_N^2	$B(E2)\uparrow^b$ s.p.u.	Structure, %
						$\nu\nu 615\downarrow - 624\downarrow$ 33
						$\pi\pi 521\uparrow - 530\uparrow$ 18
						$\nu\nu 613\uparrow - 622\uparrow$ 10
						$\nu\nu 620\uparrow + 631\downarrow$ 9
						$\nu\nu 622\uparrow - 631\uparrow$ 7
13			2.55	0.04	0.02	$(21)_8$ 13; $(21)_{12}$ 5
						$(21)_{13}$ 12
						$(21)_{19}$ 12
						$\{(22)_1, (43)_2\}$ 19
						$\{(22)_2, (43)_2\}$ 15
						$\{(54)_1, (55)_1\}$ 8
14	2.468		2.60	0.38	0.05	$(21)_{11}$ 4; $(21)_{12}$ 62
						$(21)_{17}$ 4
	$(\gamma, \gamma') : 0.36 \pm 0.03$					$\{(31)_2, (32)_1\}$ 6
	$(e, e') : 0.54 \pm 0.20$					$\{(22)_2, (43)_3\}$ 6
	[38]					$(21)_{12}$:
						$\nu\nu 615\downarrow - 624\downarrow$ 52
						$\pi\pi 633\uparrow - 642\uparrow$ 15
						$\pi\pi 523\downarrow - 532\downarrow$ 12
						$\pi\pi 521\uparrow - 530\uparrow$ 8

[a] The $B(M1)\uparrow$ are equal to $B(M1; 0^+0_{\text{g.s.}} \to 1^+1_n)$.
[b] The $B(E2)\uparrow$ are equal to $B(E2; 0^+0_{\text{g.s.}} \to 2^+1_n)$ and are given in the single-particle units.

There is no a calculated state which corresponds to the experimental 1.53 MeV state. The calculated $B(M1)$ values are larger than the $B(M1)$ values rejected in [40]. According to the present calculation, the first $K_n^\pi = 1_1^+$ state has energy of 1.18 MeV and $B(M1)\uparrow$=0.03 μ_N^2. The first 1^+ state is the lowest state due to a very low energy of the two-quasiparticle pole. The calculated $B(M1; 2^+1_1 \to 2^+0_{\text{g.s.}}) = 15 \cdot 10^{-3}$ μ_N^2 is 5.8 times as large as the rejected experimental value. The calculated $B(M1)$ values between one-phonon components of the wave functions of the initial and final states are 3–10 times as larger as the $B(M1)$ values rejected in analyses of the relevant experimental data in [40]. It is now impossible to specify the correspondence between the calculated and experimental 2^+ states unless experimental data on the K quantum numbers of these 2^+ states are obtained.

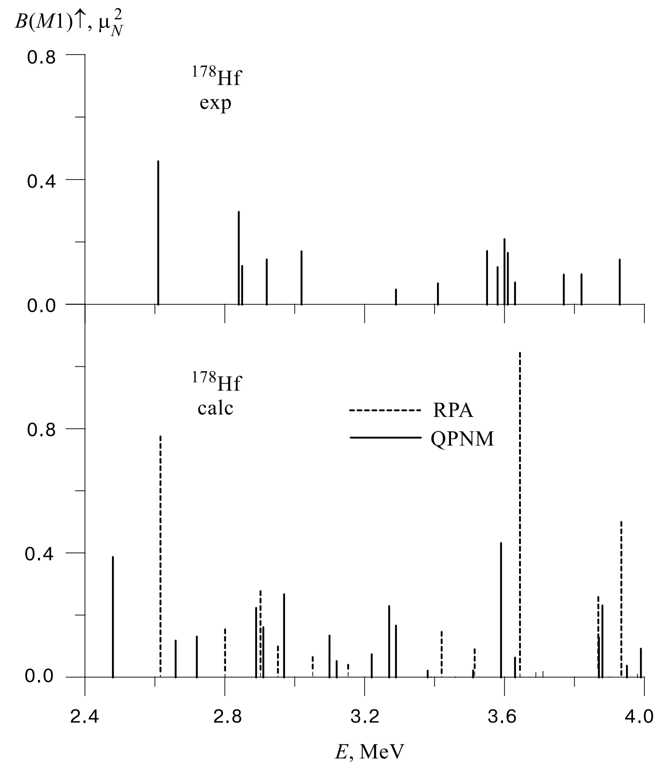

Fig. 3. Experimental, QPNM and RPA $M1$ strength distribution in ^{178}Hf. See Fig. 1 for explanatory details

It is reasonable to note that there are experimental data on relatively large $B(M1)$ values for transitions between one-phonon terms of the wave functions of the initial and final states. For example, in [42] the following $M1$ transition rates have been observed in ^{156}Gd: $B(M1; 2^-2_1 \to 2^-1_1)=8 \cdot 10^{-3}\ \mu_N^2$, $B(M1; 1^+1_2 \to 2^+0_1)=4 \cdot 10^{-2}\ \mu_N^2$ and $B(M1; 1^+1_2 \to 0^+0_2)=5 \cdot 10^{-2}\ \mu_N^2$. According to experimental data [43] in ^{168}Er, $B(M1; 3^-3_1 \to 4^-4_1)$ is $3 \cdot 10^{-2}\ \mu_N^2$, $B(M1; 3^-3_3 \to 3^-3_1)=5.8 \cdot 10^{-4}\ \mu_N^2$ and $B(M1; 3^-3_3 \to 2^-2_1) = 2.5 \cdot 10^{-4}\ \mu_N^2$.

It seems to us, it will be useful to reanalyze experimental data in [40] taking into account the $M1$ transitions. It is important to have experimental data on the K quantum number of the low-lying states in ^{238}U for performing the Coriolis coupling calculations. In this case, it will be possible to solve the disagreement between experimental data obtained in [40] and the microscopic description of vibrational states in doubly even deformed nuclei.

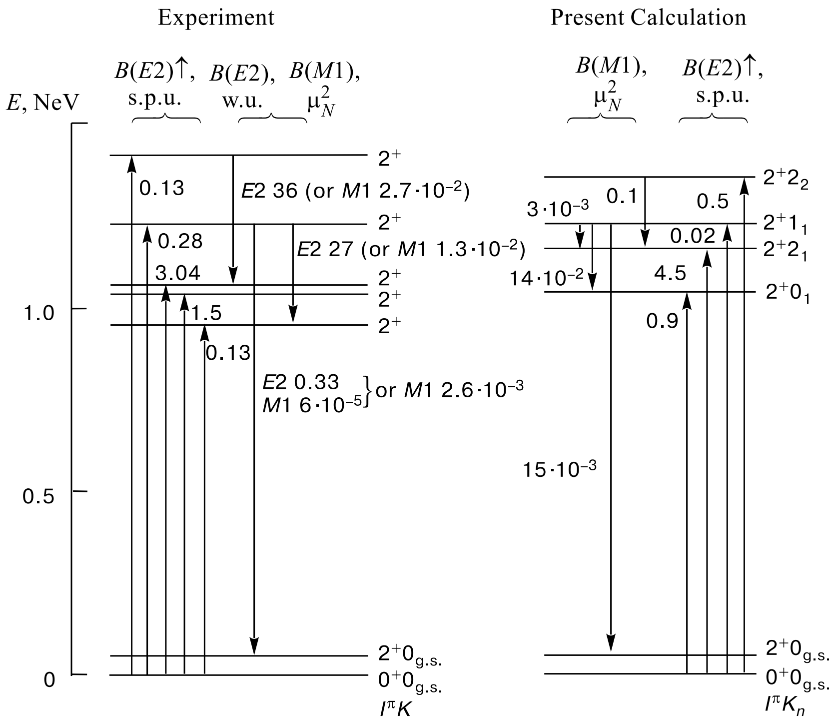

Fig. 4. Energy level diagram of the 2^+ states observed by Coulomb excitation of ^{238}U and the results of the present calculation. $(B(E2)_W = \frac{1}{4\pi}(\frac{3}{5})^2(0.12A^{1/3})^4e^2b^2)$

3.7. $K^\pi = 0^-$ **and** 1^- **States and** $E1$ **Strength Distribution.** The rich experimental data on the $E1$ strength distribution in ^{168}Er in the energy range 1.7–4.0 MeV were given in Ref. 27. We used these data for renormalization of the $E1$ effective charge. The experimental energies and $B(E1)\uparrow$ values and the calculated energies, $B(E1)\uparrow$ and $B(E3)\uparrow$ values and structure of the $K^\pi = 0^-$ and 1^- states in ^{168}Er are given in Table 5. The experimental $B(E1)\uparrow$ values in brackets mean that there is somewhat uncertain assignments of parity or/and K-quantum number. The calculated $B(E3)\uparrow$ values for excitation of the $I^\pi K_n =$ $= 3^-1_1$ and 3^-0_1 states are in agreement with the relevant experimental data. The observed $E1$ strength distribution of the $E1$, $\Delta K = 0$ strength below 3.2 MeV is somewhat stronger fragmented than the calculated ones. In general, strong fragmentation of the $E1$ strength in ^{168}Er is reasonably good described in the QPNM. As is shown in Fig. 5, the observed fragmentation of the one-phonon states with $K^\pi = 0^-$ in ^{174}Yb is relatively weak. Nevertheless, the observed $E1$, $\Delta K = 0$ strength in ^{174}Yb is stronger fragmented than the calculated ones.

Table 5. Energies, $E1$ and $E3$ strengths and structure of the QPNM $K^\pi = 0^-$ and 1^- states in ^{168}Er

K_n^π	Experiment [27]		Calculation in the QPNM			
	E_n MeV	$B(E1)\uparrow$ $e^2fm^2 \cdot 10^{-3}$	E_n MeV	$B(E1)\uparrow$ $e^2fm^2 \cdot 10^{-3}$	$B(E3)\uparrow$ s.p.u.	Structure, %
1_1^-	1.358		1.30	5.90	2.75	$(31)_1$ 95 $\{(22)_1,(33)_2\}$ 3 $(31)_1$: $\nu\nu$633↑-512↑ 81 $\nu\nu$633↑-523↓ 2
0_1^-	1.786	22.38 ± 2.51	1.85	17.3	2.80	$(30)_1$ 99 $(30)_1$: $\nu\nu$512↑-642↑ 30 $\nu\nu$514↓-633↑ 4 $\pi\pi$523↑-404↓ 3
1_2^-	1.937	0.79 ± 0.11	1.92	1.4	0.72	$(31)_2$ 96 $(31)_2$: $\nu\nu$633↑-523↓ 89 $\nu\nu$633↑-512↑ 6
0_2^-	2.137	(1.34 ± 0.25)	2.30	6.9	0.93	$(30)_2$ 99 $(30)_2$: $\nu\nu$514↓-633↑ 19 $\nu\nu$512↑-642↑ 16 $\pi\pi$523↑-404↓ 9
1_3^-	2.342	(0.52 ± 0.11)	2.28	6.0	3.31	$(31)_3$ 94 $(31)_3$: $\nu\nu$651↑-521↓ 31 $\nu\nu$633↑-512↑ 10 $\nu\nu$633↑-523↓ 7 $\nu\nu$642↑-521↑ 5 $\pi\pi$523↑-402↑ 4 $\pi\pi$532↑-411↑ 4
0_3^-	2.417	1.61 ± 0.27	2.49	0.1	$9 \cdot 10^{-3}$	$(30)_3$ 99 $(30)_3$: $\pi\pi$523↑-404↓ 32 $\nu\nu$514↓-633↑ 17
0^-	2.510	0.55 ± 0.16				

Table 5. (cont.)

K_n^π	Experiment [27]		Calculation in the QPNM			
	E_n MeV	$B(E1)\uparrow$ $e^2fm^2 \cdot 10^{-3}$	E_n MeV	$B(E1)\uparrow$ $e^2fm^2 \cdot 10^{-3}$	$B(E3)\uparrow$ s.p.u.	Structure, %
1_4^-			2.55	4.3	1.79	$(31)_4$ 91 $\{(22)_1,(33)_1\}$ 3 $\{(43)_2,(54)_1\}$ 3 $(31)_4$: $\nu\nu651\uparrow$-$521\downarrow$ 66 $\nu\nu642\uparrow$-$521\uparrow$ 3 $\pi\pi532\uparrow$-$411\uparrow$ 3
0_4^-	2.740	0.80 ± 0.14	2.72	7.0	0.85	$(30)_4$ 88 $\{(22)_1,(32)_1\}$ 4 $\{(44)_1,(54)_1\}$ 3 $(30)_4$: $\nu\nu523\downarrow$-$642\uparrow$ 28 $\nu\nu514\downarrow$-$633\uparrow$ 5 $\pi\pi523\uparrow$-$404\downarrow$ 4
1_6^-	2.849	(1.10 ± 0.15)	2.90	0.1	0.014	$(31)_5$ 95 $\{(22)_1,(33)_3\}$ 3 $(31)_5$: $\pi\pi523\uparrow$-$413\downarrow$ 92 $\nu\nu642\uparrow$-$521\uparrow$ 4
0_5^-	2.946	2.06 ± 0.27	3.03	5.3	0.79	$(30)_5$ 86; $(30)_4$ 3 $(30)_6$ 3 $\{(22)_1,(32)_1\}$ 7 $(30)_5$: $\nu\nu523\downarrow$-$642\uparrow$ 18 $\nu\nu514\downarrow$-$633\uparrow$ 10
1_7^-	2.975	(0.84 ± 0.15)	3.07	0.1	0.13	$(31)_6$ 37; $(31)_7$ 5 $(31)_8$ 4; $(31)_{10}$ 8 $(31)_{12}$ 6 $\{(20)_3,(31)_1\}$ 27 $\{(22)_1,(31)_1\}$ 5
1_8^-	3.095	(1.04 ± 0.14)	3.09	0.1	$6 \cdot 10^{-3}$	$(31)_6$ 34; $(31)_7$ 36 $(31)_8$ 7 $\{(22)_1,(31)_1\}$ 14

Table 5. (cont.)

K_n^π	Experiment [27] E_n MeV	Experiment [27] $B(E1)\uparrow$ e^{2}fm$^2 \cdot 10^{-3}$	Calculation in the QPNM E_n MeV	Calculation in the QPNM $B(E1)\uparrow$ e^{2}fm$^2 \cdot 10^{-3}$	Calculation in the QPNM $B(E3)\uparrow$ s.p.u.	Calculation in the QPNM Structure, %
0^-_6	3.181	1.96 ± 0.28	3.19	12.2	1.86	$(30)_6$ 68; $(30)_5$ 8 $(30)_4$ 5 $\{(22)_1,(32)_1\}$ 7 $\{(22)_1,(32)_2\}$ 5 $\{(44)_1,(54)_1\}$ 5
1^-_{10}	3.190	(1.16 ± 0.15)	3.15	0.4	0.08	$(31)_6$ 17; $(31)_7$ 29 $(31)_8$ 9; $(31)_{12}$ 10 $\{(20)_3,(31)_1\}$ 23 $\{(22)_1,(31)_1\}$ 5
0^-_8	3.441	(0.58 ± 0.15)	3.49	0.3	$7 \cdot 10^{-3}$	$(30)_6$ 6; $(30)_8$ 5 $\{(22)_1,(32)_1\}$ 20 $\{(22)_2,(32)_1\}$ 45 $\{(44)_1,(54)_1\}$ 14 $\{(22)_1,(32)_2\}$ 5 $\{(43)_1,(33)_2\}$ 2
1^-_{21}	3.468	(1.81 ± 0.26)	3.48	0.2	0.03	$(31)_9$ 4; $(31)_{15}$ 3 $\{(20)_1,(31)_1\}$ 76 $\{(43)_1,(54)_2\}$ 6 $\{(43)_2,(54)_1\}$ 3
0^-_9	3.480	3.64 ± 0.52	3.51	0.4	$4 \cdot 10^{-3}$	$(30)_6$ 6; $(30)_8$ 4 $\{(22)_1,(32)_1\}$ 16 $\{(22)_2,(32)_1\}$ 54 $\{(44)_1,(54)_1\}$ 9
0^-_{13}	3.505	(0.53 ± 0.24)	3.67	0.1	$4 \cdot 10^{-6}$	$(30)_7$ 6 $\{(21)_1,(31)_1\}$ 83
1^-_{22}	3.516	(1.31 ± 0.24)	3.49	0.3	0.08	$(31)_{10}$ 7; $(31)_{11}$ 3 $(31)_{12}$ 9; $(31)_{15}$ 4 $\{(43)_1,(54)_2\}$ 22 $\{(20)_3,(31)_1\}$ 20
0^-_{14}	3.703	$1.57 \pm 0.31)$	3.71	1.5	0.12	$(30)_7$ 37 $\{(21)_1,(31)_1\}$ 11 $\{(20)_3,(30)_1\}$ 38 $\{(43)_1,(33)_3\}$ 6
1^-_{35}	3.719	(1.27 ± 0.32)	3.76	1.0	0.11	$(31)_{15}$ 32 $\{(20)_1,(31)_3\}$ 17 $\{(22)_1,(31)_3\}$ 6 $\{(22)_3,(31)_1\}$ 22

A comparison between the observed fragmentation of the $E1$ strength with $\Delta K = 0$ and the calculated within the QPNM fragmentation of the $E1$ strengths with $\Delta K = 0$ and 1 in ^{166}Er, ^{172}Yb and ^{178}Hf are presented in Figs. 6, 7, and 8. The observed fragmentations of the $E1$, $\Delta K = 0$ strengths are stronger in ^{166}Er and ^{172}Yb and weaker in ^{178}Hf compared to the calculated ones.

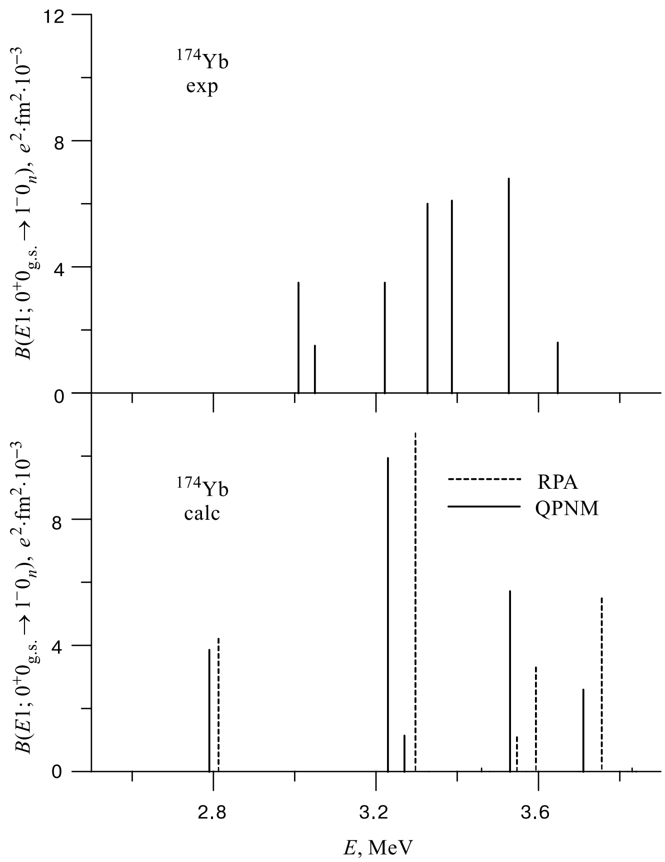

Fig. 5. Experimental, QPNM and RPA $E1$, $\Delta K = 0$ strength distribution in ^{174}Yb. See Fig. 1 for explanatory details

Recently, strong dipole excitations around 1.8 MeV in ^{238}U have been found in [39]. These dipole excitations are additional to the $M1$ strength distribution in the energy range 2.0–2.5 MeV which have been obtained in [38] by using NRF and inelastic electron scattering experiments. The results of the present calculation of the $K^\pi = 0^-$ and 1^- states in ^{238}U are given in Table 6 and Fig. 9.

In the case of negative parity of the $K = 0$ level at 1.793 MeV the $B(E1)\uparrow$ strength is $(1.4 \pm 0.5) \cdot 10^{-3}$ e^{2}fm^2. As is shown in Table 6, this level can be treated as the $I^\pi K_n = 1^- 0_3$ state at 1.85 MeV with $B(E1)\uparrow = 1.4 \cdot 10^{-3}$ e^{2}fm^2.

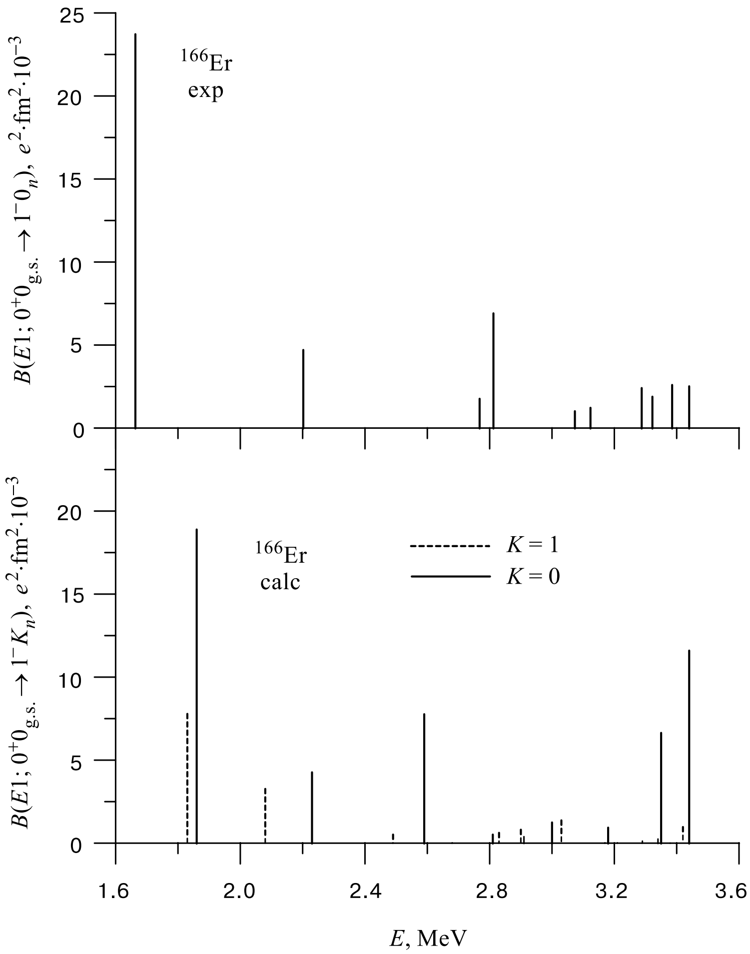

Fig. 6. Experimental $B(E1; 0^+0_{\rm g.s.} \to 1^-0_n)$ and QPNM $B(E1; 0^+0_{\rm g.s.} \to 1^-K_n)$ values in ^{166}Er. Full and dashed lines refer respectively to $K = 0$ and $K = 1$

3.8. Discussion. There are quadrupole excitations with $K = 0, 1$ and 2 in even–even deformed nuclei. Energies of the first $K_n^\pi = 0_1^+$ and 2_1^+ states are lying below the relevant first poles and their wave functions are the superposition of many two-quasiparticle components. Energies of the first $K_n^\pi = 1_1^+$ states are lying above the first poles and $B(E2)\uparrow$ values for excitations of the $I^{\pi}K_n = 2^+1_1$ states are very small. The wave functions of each first 1^+_1 state are, practically, two-quasiparticle ones. This difference is connected with approximate exclusion of the spurious 1^+ state by choosing the constant $\kappa_0^{21} \geq (\kappa_0^{21})_{\rm cr}$. The existing experimental data on the first 1^+ states in deformed nuclei support this method of exclusion of the spurious 1^+ rotational state.

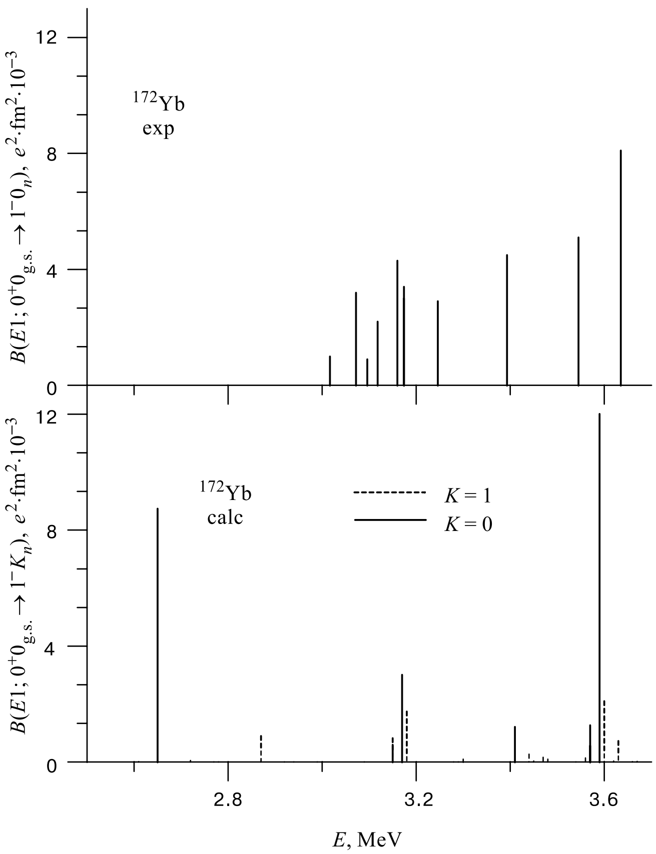

Fig. 7. Experimental $B(E1; 0^+0_{\rm g.s.}\to 1^-0_n)$ and QPNM $B(E1; 0^+0_{\rm g.s.}\to 1^-K_n)$ values in ^{172}Yb. See Fig. 6 for explanatory details

The equilibrium quadrupole deformation is responsible for splitting of subshells of the spherical basis to twice degenerated levels. Due to this splitting, the low-energy collective magnetic dipole excitations exist in deformed nuclei. Therefore, the correlation between $B(M1)\uparrow$ and $B(E2; 0^+0_{\rm g.s.}\to 2^+0_{\rm g.s.})$ takes place [45]. The energies and structure of the $K^{\pi} = 1^+$ states below 4 MeV are mostly determined by the isoscalar ph quadrupole–quadrupole interaction. An admixture of the scissors state to each intrinsic one is very small. The two-quasiparticle structure of the large one-phonon terms of the wave function (7) can be observed in the one-nucleon-transfer reaction. As is shown in [46], the large two-phonon component of the wave function (7) can be detected by fast $M1$ transition rates to the excited state differing by one-phonon with the $K^{\pi} = 1^{+}$.

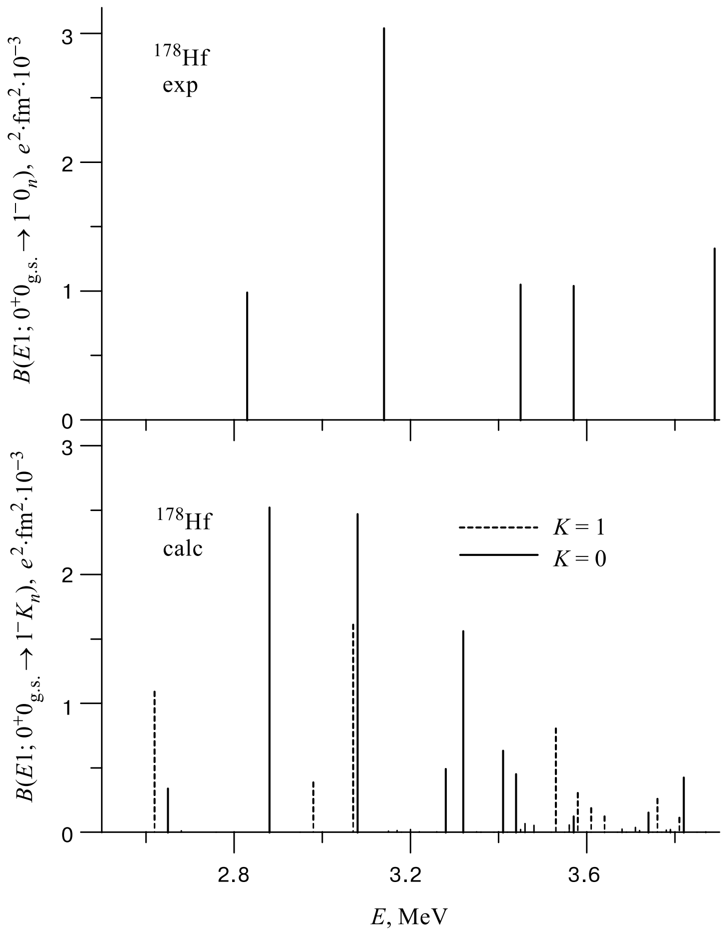

Fig. 8. Experimental $B(E1; 0^{+}0_{\rm g.s.} \to 1^{-}0_{n})$ and QPNM $B(E1; 0^{+}0_{\rm g.s.} \to 1^{-}K_{n})$ values in ^{178}Hf. See Fig. 6 for explanatory details

The experimental summed $M1$ strengths in the given energy range [47] and the results of the present calculation in several even–even deformed nuclei are given in Table 7. As is shown in Table 1, the summed in low-energy region $M1$ strengths weakly depend on the constant $\kappa_0^{21} > (\kappa_0^{21})_{\rm cr}$. Therefore, we calculated the summed $M1$ strengths in all nuclei in Table 7 with the same constants equal to $\kappa_0^{21} = 0.015$ fm^{2}MeV^{-1}, and $G^{21} = 0.8\kappa_0^{21}$. There is a very good agreement between the experimental and computed summed $M1$ strengths in all nuclei. The summed $M1$ strength calculated with the same constants κ_0^{21} and G^{21} in ^{238}U in the energy range 2.1–2.5 MeV is equal to 3.3 μ_N^2 [9], which is in agreement with the experimental values 3.19 μ_N^2 and 4.0 μ_N^2 observed respectively in the (γ,γ') and (e,e') reactions [38].

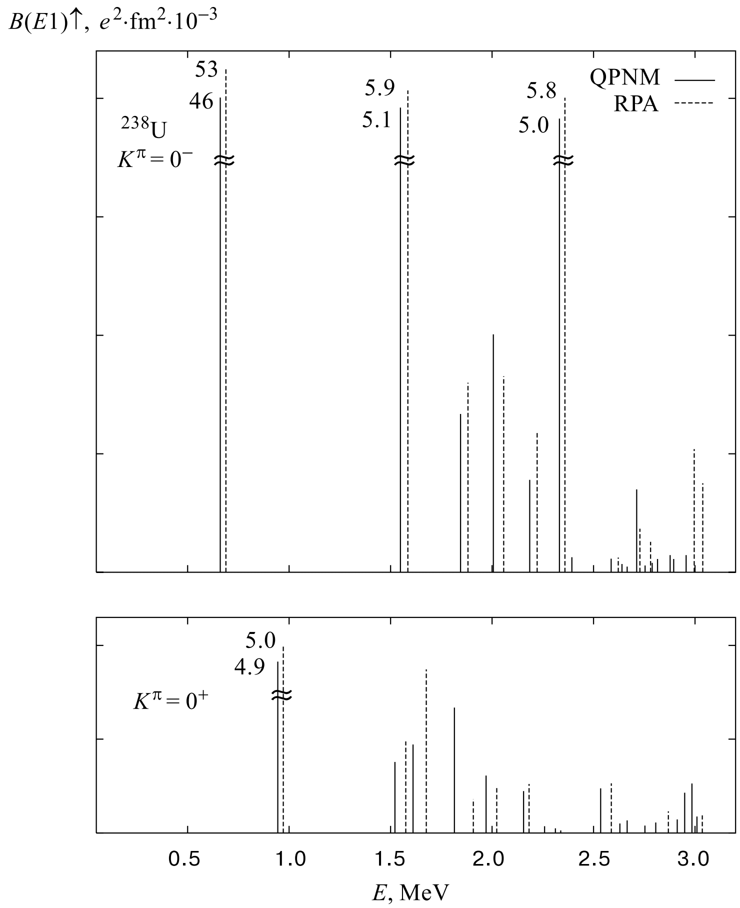

Fig. 9. $B(E1; 0^+0_{\rm g.s.}\to 1^-0_n)$ and $B(E1; 0^+0_{\rm g.s.}\to 1^-1_n)$ values in ^{238}U calculated within the RPA (dashed vertical lines) and with QPNM (solid vertical lines)

Table 6. Energies, $E1$ and $E3$ strengths and structure of the $K^\pi = 0^-$ and 1^- states in ^{238}U

	Experiment [ref]		Calculation in QPNM			
K_n^π	E_n MeV	$B(E3)\uparrow$ s.p.u. $B(E1)\uparrow$ $e^2fm^2 10^{-3}$	E_n MeV	$B(E3)\uparrow^a$ s.p.u.	$B(E1)\uparrow^b$ $e^2fm^2 10^{-3}$	Structure, %
0_1^-	0.680	$B(E3)\uparrow$=25 [44]	0.66	11.4	46	$(30)_1$ 99
		$B(E3)\uparrow$=24 [40]				$(30)_1$:
						$\nu\nu743\uparrow-624\downarrow$ 22
		$B(E1)\uparrow$=44 [44]				$\pi\pi521\uparrow-651\uparrow$ 4
		$B(E1)\uparrow$=27 [40]				$\nu\nu752\uparrow-622\uparrow$ 3
						$\pi\pi523\downarrow-642\uparrow$ 3
1_1^-	0.931	$B(E3)\uparrow$=8.1 [44]	0.95	7.8	4.9	$(31)_1$ 99
		$B(E3)\uparrow$=7.8 [40]				$(31)_1$:
						$\nu\nu743\uparrow-622\uparrow$ 71
						$\nu\nu734\uparrow-624\downarrow$ 3
						$\pi\pi521\uparrow-642\uparrow$ 3
1_2^-			1.51	1.4	0.7	$(31)_2$ 95
						$(31)_2$:
						$\pi\pi523\downarrow-651\uparrow$ 67
						$\nu\nu734\uparrow-624\downarrow$ 3
0_2^-			1.56	1.3	5.1	$(30)_2$ 99
						$(30)_2$:
						$\nu\nu743\uparrow-624\downarrow$ 25
						$\pi\pi523\downarrow-642\uparrow$ 11
						$\nu\nu752\uparrow-622\uparrow$ 5
1_3^-			1.58	1.4	0.9	$(31)_3$ 87; $(31)_4$ 4
						$(31)_3$:
						$\pi\pi523\downarrow-651\uparrow$ 31
						$\nu\nu734\uparrow-624\downarrow$ 27
						$\nu\nu743\uparrow-622\uparrow$ 12
0_3^-	(1.793)	$B(E1)\uparrow$=1.4 [39]	1.80	0.28	1.3	$(30)_3$ 99
						$(30)_3$:
						$\pi\pi523\downarrow-642\uparrow$ 32
						$\nu\nu752\uparrow-622\uparrow$ 12
1_4^-			1.81	2.2	1.3	$(31)_3$ 8; $(31)_4$ 83
						$\{(21)_1, (32)_1\}$ 3
						$(31)_4$:
						$\nu\nu734\uparrow-624\downarrow$ 49

Table 6. (cont.)

K_n^π	Experiment [ref] E_n MeV	$B(E3)\uparrow$ s.p.u. $B(E1)\uparrow$ $e^2fm^2 10^{-3}$	Calculation in QPNM E_n MeV	$B(E3)\uparrow^a$ s.p.u.	$B(E1)\uparrow^b$ $e^2fm^2 10^{-3}$	Structure, %
						$\nu\nu743\uparrow-633\downarrow$ 38 $\pi\pi530\uparrow-402\downarrow$ 4
1_5^-			2.97	1.1	0.6	$(31)_4$ 2; $(31)_5$ 94 $(31)_5$: $\nu\nu743\uparrow-633\downarrow$ 47 $\pi\pi530\uparrow-402\downarrow$ 28 $\nu\nu734\uparrow-624\downarrow$ 8
0_4^-			2.04	0.37	2.0	$(30)_4$ 97 $(30)_4$: $\nu\nu752\uparrow-622\uparrow$ 23 $\pi\pi530\uparrow-660\uparrow$ 20
1_6^-			2.14	0.44	0.6	$(31)_6$ 96 $(30)_6$: $\pi\pi530\uparrow-402\downarrow$ 58 $\nu\nu752\uparrow-624\downarrow$ 9 $\pi\pi521\uparrow-660\uparrow$ 6 $\pi\pi523\uparrow-402\uparrow$ 6 $\pi\pi530\uparrow-651\uparrow$ 6
0_5^-			2.19	0.13	0.6	$(30)_5$ 98 $(30)_5$: $\nu\nu743\uparrow-613\uparrow$ 25 $\pi\pi530\uparrow-660\uparrow$ 17
1_7^-			2.20	$2\cdot10^{-3}$	0.02	$(31)_7$ 99 $(31)_7$: $\pi\pi530\uparrow+660\uparrow$ 99
1_8^-			2.25	0.13	0.05	$(31)_8$ 89; $(31)_9$ 5 $\{(32)_1,(43)_2\}$ 2 $(31)_8$: $\nu\nu752\uparrow-624\downarrow$ 73 $\pi\pi530\uparrow-651\uparrow$ 23
1_9^-			2.30	0.03	0.03	$(31)_8$ 6; $(31)_9$ 60 $(31)_{10}$ 4 $\{(32)_1,(21)_1\}$ 24 $(31)_9$: $\pi\pi530\uparrow-651\uparrow$ 62

Table 6. (cont.)

K_n^π	Experiment [ref] E_n MeV	$B(E3)\uparrow$ s.p.u. $B(E1)\uparrow$ e^{2}fm$^2 10^{-3}$	Calculation in QPNM E_n MeV	$B(E3)\uparrow^a$ s.p.u.	$B(E1)\uparrow^b$ e^{2}fm$^2 10^{-3}$	Structure, %
						$\pi\pi521\uparrow-660\uparrow$ 15 $\nu\nu752\uparrow-624\downarrow$ 11
1^-_{10}			2.31	0.03	0.007	$(31)_9$ 22; $(31)_{10}$ 2 $\{(32)_1,(21)_1\}$ 67
0^-_6			2.32	0.59	5.0	$(30)_6$ 93 $\{(31)_1,(21)_1\}$ 3 $(30)_6$: $\nu\nu743\uparrow-613\uparrow$ 20 $\pi\pi521\uparrow-651\uparrow$ 13 $\pi\pi530\uparrow-660\uparrow$ 5
0^-_7			2.34	0.01	0.12	$(30)_6$ 3 $\{(31)_1,(21)_1\}$ 96
1^-_{11}			2.35	0.04	0.03	$(31)_9$ 9; $(31)_{10}$ 75 $\{(31)_1,(22)_3\}$ 6 $(31)_{10}$: $\pi\pi521\uparrow-660\uparrow$ 55 $\pi\pi523\downarrow-402\downarrow$ 42
1^-_{12}			2.49	$4\cdot10^{-3}$	0.02	$(31)_{11}$ 87 $\{(32)_1,(43)_1\}$ 6 $(31)_{11}$: $\nu\nu743\uparrow-615\downarrow$ 99
1^-_{13}			2.52	0.47	0.48	$(31)_{10}$ 4; $(31)_{12}$ 44 $(31)_{16}$ 3 $\{(32)_1,(43)_1\}$ 10 $\{(32)_1,(43)_2\}$ 22 $\{(31)_1,(22)_3\}$ 8 $(31)_{12}$: $\pi\pi521\uparrow-642\uparrow$ 50 $\pi\pi523\downarrow-402\downarrow$ 26 $\pi\pi521\uparrow-660\uparrow$ 10

[a] The $B(E3)\uparrow$ are equal to $B(E3; 0^+0_{\rm g.s.}\to 3^- K_n)$ and are given in the single-particle units.

[b] The $B(E1)\uparrow$ are equal to $B(E1; 0^+0_{\rm g.s.}\to 1^- K_n)$ and are given in e^{2}fm$^2\cdot 10^{-3}$.

The spin $M1$ strength dominates at energies above 6 MeV. The total $M1$ strength summed up to 30 MeV in ^{168}Er is practically equal to the sum of the orbital and spin $M1$ parts.

Table 7. Summed $M1$ strengths in even-even nuclei

Nucleus	E [MeV]	$\sum B(M1)\uparrow[\mu_N^2]$ Exp.[[47]]	$\sum B(M1)\uparrow[\mu_N^2]$ calc. QPNM
^{156}Gd	2.7–3.7	2.73	2.95
^{158}Gd	2.7–3.7	3.39	3.41
^{160}Gd	2.7–3.7	2.97	2.86
^{160}Dy	2.7–3.7	2.42	2.46
^{162}Dy	2.7–3.7	2.49	2.60
^{164}Dy	2.7–3.7	3.18	2.92
^{166}Er	2.4–3.7	2.67	2.51
^{168}Er	2.4–3.7	2.82	2.87
^{172}Yb	2.4–3.7	1.94	2.25
^{174}Yb	2.4–3.7	2.70	2.84
^{178}Hf	2.4–3.7	2.04	2.30

There are low-lying collective octupole states with $K^\pi = 0^-$ and 1^- in most even–even deformed nuclei. In contrast with strongly dipole exciting $I^\pi 0_n = = 1^- 0_1$ states in many nuclei no indication of these states was found in ^{178}Hf [37]. According to calculation in [48] within the QPNM, the first $K^\pi_n = 0^-_1$ state in ^{178}Hf has energy around 2 MeV and $B(E1; 0^+0_{g.s.} \to 1^-0_1) = 0.8 \cdot 10^{-3}$ e^{2}fm^2. The calculated reduced $E1$ transitions to the first $K^\pi_n = 1^-_1$ 1.31 MeV and second 1^-_2 1.513 MeV states are $0.14 \cdot 10^{-3}$ e^{2}fm^2 and $0.3 \cdot 10^{-3}$ e^{2}fm^2, respectively.

The existence of strongly dipole excited $K^\pi = 0^-$ states in the energy range 2–4 MeV is a common phenomenon in even–even deformed nuclei. Only a few $E1$ transitions from the ground state to the $K^\pi = 1^-$ states were observed. Therefore, we compare the experimental data with the computed ones for transitions to the $K^\pi = 0^-$ states. The experimental and computed summed $E1$ strengths in the given energy range are given in Table 8. Agreement between experimental and computed data is quite good. The large summed $E1$ strengths in ^{166,168}Er are due to very large $B(E1)$ values for transitions to the first $K^\pi_n = 0^-_1$ states. Strong $E1$ transitions in ^{172}Yb are shifted to higher excitations.

According to the experimental data [37], in ^{178}Hf comparably strong excited states are missing and summed $E1$ strength in the energy range 2–4 MeV is decreased compared to deformed nuclei of the rare-earth region. We correctly described this decreasing. The summed $E1$ strength decreases in ^{178}Hf due to the small $E1$-matrix elements between the single-particle states near the Fermi levels in the neutron and proton systems.

The one-phonon state with $K^\pi = 1^+$ at 1.8 MeV is fragmented to two levels observed in ^{238}U due to the quasiparticle–phonon interactions. The strength of the state at 2.18 MeV is $B(M1)\uparrow = 1.60\ \mu_N^2$, which is larger than the relevant RPA value due to coherent enhance of the contribution of the fifth, sixth and eighth phonons. Such a coherence goes against the experimental situation. Strong fragmentation of the one-phonon states takes place at the excitation energy above 2.3 MeV. The calculated spectra agree rather well with the experimental data.

Table 8. Summed $E1$ strengths in even-even deformed nuclei

Nucleus	E [MeV]	$\sum_n B(E1; 0^+0_{\mathrm{g.s.}} \to 1^-0_n)$ [e^{2}fm$^2 \cdot 10^{-3}$] exp.	ref.	calc. QPNM
^{156}Gd	2.5–3.3	9.5	[49]	10.5
^{158}Gd	2.8–3.9	11.2	[49]	10.1
^{160}Gd	2.0–3.2	10.2	[50]	7.7
^{162}Dy	2.5–3.0	9.0	[51]	10.0
^{164}Dy	2.0–4.0	30.0	[52]	36.0
^{166}Er	1.6–3.5	52.0	[27]	52.0
^{168}Er	1.7–4.0	52.0	[27]	52.0
^{172}Yb	2.0–3.7	49.1	[33]	34.0
^{174}Yb	3.0–3.7	23.0	[33]	19.5
^{178}Hf	2.0–4.0	12.7	[37]	12.0

We have also calculated nonrotational states with $K^\pi = 1^+, 0^-$ and 1^- in ^{240}Pu in addition to other states calculated in [41]. The overlap of the scissor with the low-lying 1^+ states, the dominance of the orbital part of $B(M1)\uparrow$ values and the fragmentation of the $K^\pi = 1^+$ one-phonon states in ^{240}Pu are similar to ^{238}U.

The total $E2$ strength for the excitation of the $I^\pi K = 2^+1$ states in ^{238}U below 2.5 MeV is about two times as small as ones for the excitation of the $I^\pi K = 2^+0$ states and is about an order of magnitude smaller than the total $E2$ strength for the excitation of the $I^\pi K = 2^+2$ states. According to the present calculation, the fragmentation of the one-phonon states in ^{238}U and ^{240}Pu with energies below 2.3 MeV is as weak as in the rare-earth nuclei. The calculated summed $E1$ strength for the levels with $K^\pi = 0^-$ is about three times as large as for the levels with $K^\pi = 1^-$ at energies below 2.5 MeV.

According to the QPNM calculations [12], there is a strong correlation between the largest $B(E1)\uparrow$ and $B(E3)\uparrow$ values with excitations of the $I^\pi K = 1^-0$, 1^-1, 3^-0, and 3^-1 states. The calculated correlation coefficient r between the $B(E1)\uparrow$ and $B(E3)\uparrow$ values equals 0.987 in ^{160}Gd, ^{160,162,164}Dy [12] and 0.998

in ^{238}U and ^{240}Pu [9] for the $K^\pi = 0^-$ states and 0.910 in ^{160}Gd, ^{160,162,164}Dy, and 0.995 in ^{238}U and ^{240}Pu for the $K^\pi = 1^-$ states. According to our calculation [10], the coefficient r equals 0.96 in ^{166}Er for the $K^\pi = 0^-$ and 1^- states and 0.75 for the $K^\pi = 0^-$ states and 0.87 for the $K^\pi = 1^-$ in ^{172}Yb, ^{174}Yb, and ^{178}Hf. It means that the correlation between $B(E1)\!\uparrow$ and $B(E3)\!\uparrow$ values is a general property in even–even deformed nuclei.

Let us consider the intensities of the $M1$ and $E1$ transitions to excited states between 2 MeV and 4 MeV in even–even deformed nuclei. According to the experimental data [27], the $M1$ and $E1$ reduced widths in ^{168}Er summed in the energy range 2–4 MeV are the following:

$$\sum_n \Gamma_0^{\rm red}(M1; 0^+0_{\rm g.s.} \to 1^+1_n) = 11.6\ {\rm meV/MeV^3},$$

$$\sum_n \Gamma_0^{\rm red}(E1; 0^+0_{\rm g.s.} \to 1^-0_n) = 10.1\ {\rm meV/MeV^3}.$$

The $M1$ and $E1$ reduced widths are quite similar. In the experiments on ^{168}Er only three weaker $E1$ transitions with a tentative $K = 1$ assignment have been detected.

Table 9. Calculated in the QPNM $M1$ and $E1$ reduced widths, summed in the energy range 2–4 MeV

Nucleus	$\sum_n \Gamma^{\rm red}(M1;$ $0^+0_{\rm g.s.} \to 1^+1_n)$ meV/MeV^3	$\sum_n \Gamma^{\rm red}(E1;$ $0^+0_{\rm g.s.} \to 1^-0_n)$ meV/MeV^3	$\sum_n \Gamma^{\rm red}(E1;$ $0^+0_{\rm g.s.} \to 1^-1_n)$ meV/MeV^3
^{160}Gd	17.5	6.0	4.0
^{160}Dy	14.4	12.1	4.1
^{162}Dy	18.4	14.8	4.2
^{164}Dy	19.2	12.6	3.1
^{166}Er	12.8	13.3	3.6
^{168}Er	15.9	12.9	5.0
^{172}Yb	14.6	12.9	5.7
^{174}Yb	16.5	10.1	4.1
^{178}Hf	13.7	4.2	3.1

For comparison of the intensities of the $M1$ and $E1$ transitions in even–even deformed nuclei, we computed the $M1$ and $E1$ reduced widths. The results of the calculations within the QPNM of the $M1$ and $E1$ with $\Delta K = 0$ and $\Delta K = 1$ widths summed in energy range 2–4 MeV are presented in Table 9. The computed summed $M1$ and $E1$ reduced widths are close to one another. It means that the intensity of the $E1$ and $M1$ transitions is quite similar in the energy range 2–4 MeV.

Table 10. Calculated decay rates from the levels to the one-phonon and ground states in ^{238}U

Initial state			Final state				
$I^\pi K_n$	E_n (MeV)	Structure, %	$E1$ or $M1$	$I^\pi K_n$	E_n (MeV)	$B(E1)$ $\mathrm{e^2fm^2} \cdot 10^{-3}$ or $B(M1)$ μ_N^2	Decay rate (sec)
3^-0_1	0.71	$(30)_1$ 99	$E1$	$2^+0_{\text{g.s.}}$	0.045	20	$1 \cdot 10^{13}$
3^-1_1	1.01	$(31)_1$ 99	$E1$	$2^+0_{\text{g.s.}}$	0.045	1.4	$2 \cdot 10^{12}$
2^+1_1	1.21	$(21)_1$ 97	$M1$	$2^+0_{\text{g.s.}}$	0.045	$15 \cdot 10^{-3}$	$4 \cdot 10^{11}$
			$M1$	2^+2_1	1.060	$3 \cdot 10^{-3}$	$2 \cdot 10^{8}$
			$M1$	2^+0_1	0.97	$14 \cdot 10^{-2}$	$4 \cdot 10^{10}$
2^+2_2	1.35	$(22)_2$ 96	$M1$	2^+2_1	1.06	0.10	$8 \cdot 10^{10}$
1^+1_4	1.97	$(21)_2$ 14	$E1$	2^-2_1	1.13	7	$6 \cdot 10^{12}$
		$(21)_5$ 16					
		$(21)_6$ 2					
		$(21)_8$ 15					
		$\{(30)_1, (32)_1\}$ 48					
			$M1$	$0^+0_{\text{g.s.}}$	0.00	0.12	$1 \cdot 10^{13}$
0^+0_8	2.07	$(20)_6$ 34	$E1$	1^-1_1	0.93	15	$3 \cdot 10^{13}$
		$(20)_8$ 18					
		$\{(31)_1, (31)_1\}$ 36					
1^-1_{28}	2.85	$(31)_{16}$ 33	$E1$	2^+2_1	1.06	0.9	$8 \cdot 10^{12}$
		$(31)_{17}$ 4					
		$\{(31)_1, (22)_1\}$ 7					
		$\{(31)_2, (22)_1\}$ 19					
		$\{(31)_3, (22)_1\}$ 12					
			$E1$	$0^+_{\text{g.s.}}$	0.00	0.01	$3 \cdot 10^{11}$
1^-0_{25}	3.06	$(30)_{10}$ 6	$M1$	1^-1_1	0.93	0.04	$7 \cdot 10^{12}$
		$(30)_{12}$ 10					
		$\{(21)_3, (31)_1\}$ 21					
		$\{(20)_2, (30)_1\}$ 34					
		$\{(22)_1, (32)_1\}$ 22					
			$E1$	$0^+_{\text{g.s.}}$	0.00	0.23	$1 \cdot 10^{13}$
1^+1_{50}	3.08	$(21)_{19}$ 28	$M1$	2^+2_1	1.06	0.2	$3 \cdot 10^{13}$
		$\{(21)_2, (22)_1\}$ 15					
		$\{(22)_1, (43)_2\}$ 6					
		$\{(22)_1, (43)_3\}$ 3					
		$\{(22)_2, (43)_3\}$ 4					
		$\{(43)_2, (44)_2\}$ 29					
			$M1$	$0^+_{\text{g.s.}}$	0.00	0.03	$2 \cdot 10^{13}$

According to experimental data, the $B(E1; 0^+0_{\rm g.s.} \rightarrow 1^-0_n)$ values are larger than the $B(E1; 0^+0_{\rm g.s.} \rightarrow 1^-1_n)$ values in several even-even deformed nuclei. The summed $E1$ reduced widths with $\Delta K = 0$ and $\Delta K = 1$ are given in Table 9. As is shown in Table 9, the summed reduced widths for $E1$ transitions to the levels with $K^\pi = 0^-$ are about three times as large as to the levels with $K^\pi = 1^-$. It is in agreement with the conclusion made in Ref. 12. A situation is changing in ^{178}Hf where the $E1$, $\Delta K = 0$ summed reduced width strongly decreases.

The calculation within the QPNM has shown [46] that there are fast $E1$ and $M1$ transitions between large components of the wave functions of the initial and final states differing by the octupole ($K^\pi = 0^-$ or 1^-) or quadrupole ($K^\pi = 1^+$) phonon in several well-deformed doubly even nuclei in the rare-earth region. Fast γ-ray transitions between excited states can be treated as evidence of order in deformed nuclei at excitation energy less than 8 MeV.

Several typical cases of the $E1$ and $M1$ decay rates per second into excited and ground states in ^{238}U are presented in Table 10. As is shown in Table 10, there are fast $E1$ and $M1$ transitions between excited states if the wave function of the initial state has a relatively large two-phonon term consisting of the octupole phonon with $K^\pi = 0^-$ or 1^- or has a quadrupole phonon with $K^\pi = 1^+$ and another phonon that is the same as the phonon of the wave function of the final state. The large two-phonon component of the wave function of an excited state can be observed experimentally through the fast $E1$ and $M1$ transitions. Nevertheless, the intensity of the K-allowed γ-ray transitions from the levels below 2.5 MeV to the ground states are larger than to excited states.

The fast $E1$ and $M1$ transitions between excited states are specific of deformed nuclei. This is a very important property of deformed nuclei. It is difficult to expect such fast $E1$ and $M1$ transitions in spherical nuclei.

4. DIPOLE STRENGTH DISTRIBUTION AT 4–12 MeV ENERGY REGION

4.1. Calculation Details. Now we will discuss dipole strength distribution in the intermediate energy range 4–12 MeV for the rare-earth nuclei ^{154}Sm, ^{168}Er, ^{178}Hf, and for ^{238}U.

The parameters of the Woods–Saxon potential, including the deformation parameters β_2 and β_4, were the same as in Sect. 3. The single-particle spectrum was taken from the bottom of the potential well up to +15 MeV.

The $K^\pi = 1^+$ states were calculated in RPA using isoscalar and isovector ph and pp quadrupole–quadrupole interactions as well as isoscalar and isovector ph spin–spin potentials. In ^{168}Er, ^{178}Hf, and ^{238}U we chose the value $\kappa_0^{21} = 0.015$ fm^{2}MeV^{-1} as in Sect. 3. In ^{154}Sm, instead, we used $\kappa_0^{21} = 0.016$ fm^{2}MeV^{-1} since the critical value was $(\kappa_0^{21})_{\rm cr} = 0.0158$ fm^{2}MeV^{-1}.

The $K^\pi = 0^-$ and 1^- states were computed, also in RPA, using ph and pp isoscalar and isovector octupole–octupole interactions as well as a ph isovector dipole–dipole potential. We used the same ph dipole and octupole constants κ_1^{1K}, κ_0^{3K}, κ_1^{3K} as in Sect. 3.

4.2. $M1$ **Strength Distribution.** The $M1$ strengths were computed using bare orbital gyromagnetic factors and an effective spin factor $g_s^{\rm eff} = 0.7 g_s^{\rm free}$. As shown elsewhere [8, 10], the $M1$ transitions in the low-energy range (2–4 MeV) are mainly of orbital nature. The spin motion is nonetheless important, since its small contribution adds coherently to the dominant orbital part. The contribution of the scissors components of each one-phonon state to each transition is small [10]. Because of coherent effects, however, the scissors contribution to the total $M1$ strength is considerably large.

Orbital, spin and total $M1$ strength distributions in the energy range 4–12 MeV were computed for ^{154}Sm, ^{168}Er, ^{178}Hf, and ^{238}U. The contribution of the scissors part to the $M1$ strength was also estimated. The most meaningful results are illustrated in Figs. 10–16.

We first analyzed the role of the orbital motion and of the scissors correlation in the energy region 4–12 MeV. For illustrative purposes it is enough to show the results only for ^{154}Sm (Fig. 10). The $M1$ strength due to the orbital motion has its maximum around 4.8 MeV and then decreases with the energy. By contrary, the contribution of the scissors part to the orbital $M1$ strength is very small all over the energy interval. Indeed, the computed scissors $M1$ strength, summed in bins of 0.2, 0.5 and 1.0 MeV, is practically the same and is equal to 0.2–0.3 μ_N^2. It means that the scissors amplitudes are not coherent.

Orbital, spin and total $M1$ strength distributions in ^{154}Sm, summed in bins of 0.2 MeV, instead of 1.0 MeV as in [10], are shown in Fig. 11. On the whole, the orbital contribution is considerably smaller than the spin part (Table 11). Nonetheless, the orbital motion plays a noticeable role in shaping the strength distribution. Indeed, because of the destructive interference with the spin motion all over the energy interval (Fig. 11), the total $M1$ strength distribution exhibits some deep minima.

Quite noticeable is the two-peak structure. The two peaks, however, are shifted upward by about 1 MeV with respect to the experimental bumps (Fig. 12) [16]. Also evident is the minimum in between. This would be consistent with the new (γ, γ') results, Fig. 13 [18]. However, like the peaks, also the computed minimum is shifted upward with respect to the experimental one. For the rest, we may observe some small strength distributed up to 6.5 MeV and then another deep minimum. Above ~ 9 MeV the strength is quite small. Only around 12 MeV a small bump may be noticed.

The $M1$ strength concentrated in the peak around 7.1 MeV is due to the contributions of the $\nu\nu 514\uparrow - 514\downarrow$ $(1h_{11/2} - 1h_{9/2})$ and $\pi\pi 404\uparrow - 404\downarrow$ $(1g_{9/2} - 1g_{7/2})$ configurations.

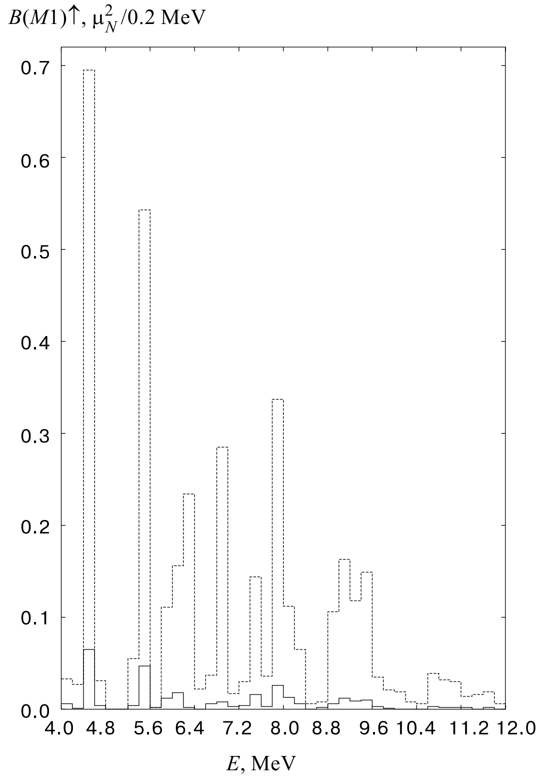

Fig. 10. Orbital (dashed line) and scissors (full line) $M1$ strength distributions in ^{154}Sm calculated in RPA

Also the $\pi\pi 532\uparrow - 532\downarrow$ and $541\uparrow - 530\uparrow$ $(1h_{11/2} - 1h_{9/2})$ configurations contribute. The other peak in the energy range 8.6–8.8 MeV is promoted by the $\nu\nu 505\uparrow - 505\downarrow$ $(1h_{11/2} - 1h_{9/2})$ and, partly, by $\pi\pi 651\uparrow - 420\uparrow$ $(2d_{5/2} - 2dg_{3/2})$ configurations. Clearly, according to our results, the two peaks cannot be considered as separate excitations of protons and neutrons. Each peak in fact gets contributions from two-quasiproton as well as two-quasineutron configurations. On the other hand, the two peaks cannot be ascribed to separate isoscalar and isovector excitations either. Indeed, the spectrum resulted to be rather insensitive to variation of the isovector coupling constant. More specifically, when equal isoscalar and isovector coupling constants were employed, the total magnitude of the $M1$ strength remained practically unchanged and its distribution was little affected, since the variation induced on each bin was always less than 10%.

As we move to ^{168}Er (Fig. 14) and ^{178}Hf (Fig. 15), the fragmentation of the $M1$ strength gets more pronounced. In ^{168}Er we still observe two prominent

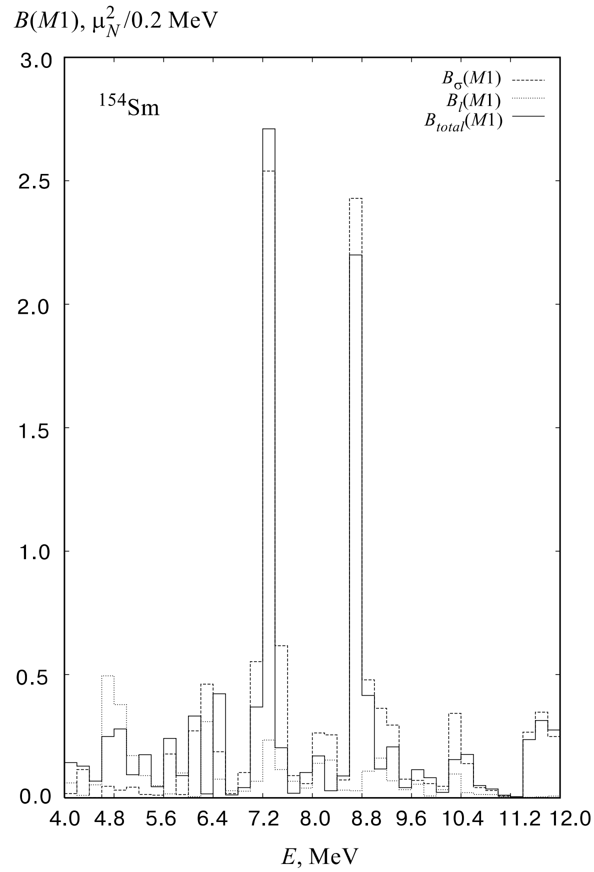

Fig. 11. RPA $M1$ strength distributions, summed in bins of 0.2 MeV, are shown for ^{154}Sm in the 4–12 MeV energy range. The spin $B_\sigma(M1)$ (upper part), orbital $B_l(M1)$ (middle part) and total $B_{\rm total}(M1)$ (lower part) contributions are plotted

peaks, but the strength is distributed at least in four regions. In ^{178}Hf only a dominant peak survives. As in ^{154}Sm, also in these nuclei orbital and spin motions interfere destructively. Some peculiarities may also be noticed. While ^{168}Er exhibits a rather broad bump above 10 MeV, the ^{178}Hf nucleus gets practically no strength above $\sim$ 9 MeV. In ^{238}U (Fig. 16) most of the strength is concentrated between ~ 5.5 and ~ 10 MeV and is compatible with a two-bump structure. Also in this nucleus the effect of the destructive interference between the orbital and spin amplitudes is quite noticeable.

The orbital $\sum B_l(M1)\!\uparrow$, spin $\sum B_\sigma(M1)\!\uparrow$ and total $\sum B_{\rm total}(M1)\!\uparrow$ $M1$ strengths, summed over the energy range 4–12 MeV for ^{154}Sm, ^{168}Er, and ^{178}Hf

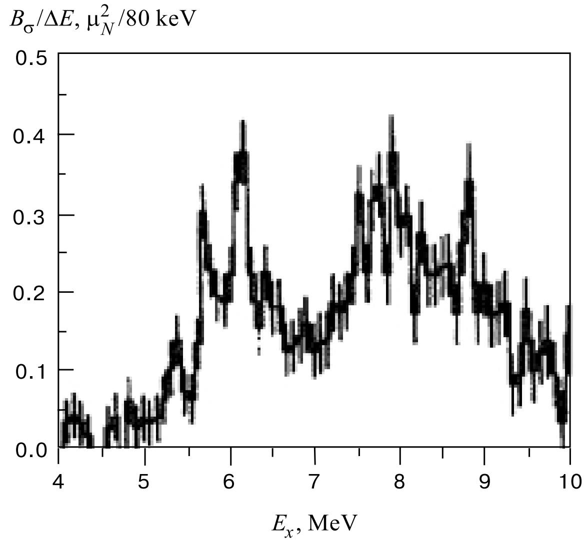

Fig. 12. The experimental $M1$ strength distribution obtained by (p,p′) scattering experiments

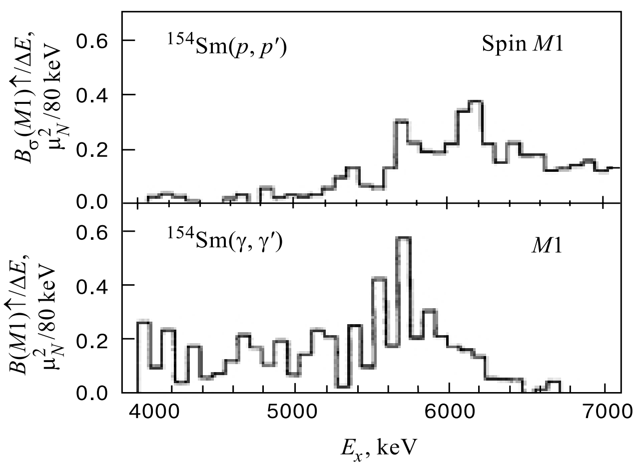

Fig. 13. The experimental $M1$ strength distribution obtained in (p,p′) scattering and (γ, γ') experiments

and over 3–11 MeV for ^{238}U, are given in Table 11. The downward shift of the lower limit in ^{238}U was dictated by the fact that the low-energy strength is concentrated in the energy range 1.5–3.0 MeV [9]. The spin part of the $M1$ strength is dominating. The orbital part of the $M1$ strength in the energy range 4–12 MeV is small. Nevertheless, we have seen that the destructive interference

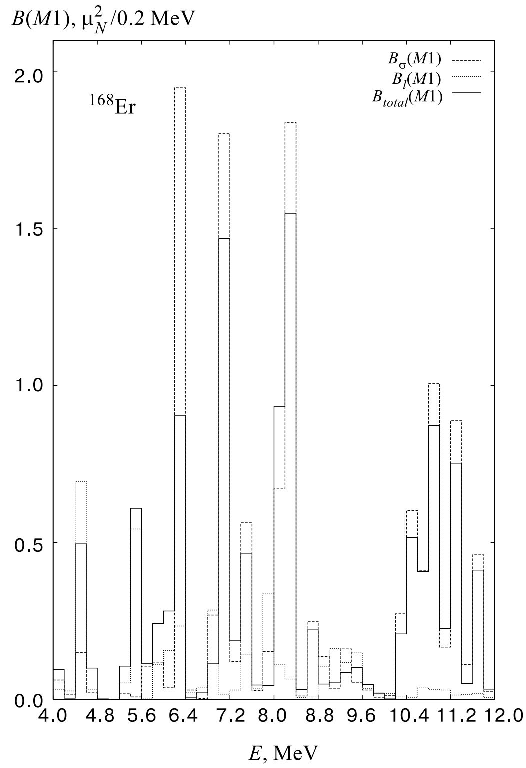

Fig. 14. The same as in Fig. 11 but for ^{168}Er

of the orbital and spin $M1$ components affects considerably the $M1$ strength distribution specially in the energy range 6–9 MeV. This destructive interference is clearly demonstrated in Table 11 for all computed nuclei.

Table 11. Summed orbital, spin and total $M1$ strengths in ^{154}Sm, ^{168}Er, ^{178}Hf, and ^{238}U

Nucleus	E [MeV]	$\sum B_l(M1)\uparrow$ $[\mu_N^2]$	$\sum B_\sigma(M1)\uparrow$ $[\mu_N^2]$	$\sum B_{\text{total}}(M1)\uparrow$ $[\mu_N^2]$
^{154}Sm	4–12	3.3	11.9	10.8
^{168}Er	4–12	3.7	12.6	11.8
^{178}Hf	4–12	3.8	12.3	11.7
^{238}U	3–11	3.7	14.4	13.4

4.3. $E1$ Strength Distribution. The calculation of the $E1$ strength in the region 3–7 MeV poses the delicate problem of the choice of the effective charge.

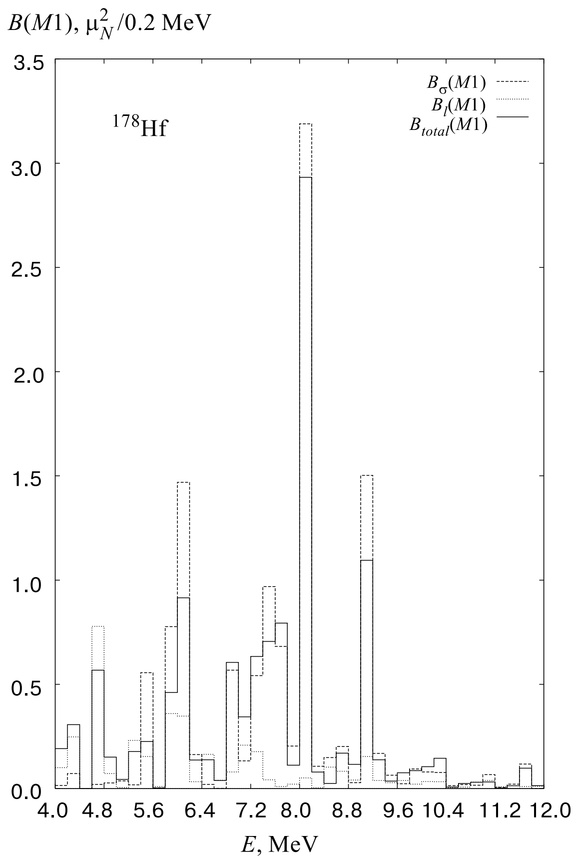

Fig. 15. The same as in Fig. 11 but for ^{178}Hf

The GDR, which covers the region above 7 MeV, is well reproduced by just using a bare charge.

It is not obvious which effective charge should be used for the $E1$ transitions in the intermediate region under investigation. We decided to use the same effective charge adopted for the low-energy region by choosing the factor $(1+\chi)^2 = 0.2$ to calculate the $B(E1; 0^+0_{\rm g.s.}\to 1^-0_n)$ and $B(E1; 0^+0_{\rm g.s.}\to 1^-1_n)$ values for the energy range 3.6–7.6 MeV (2.6–6.6 MeV for ^{238}U). This is the best choice for our purposes. One of our aims is to explore if $E1$ transitions occur in the intermediate region under investigation. By using a severely quenched effective charge, we may have at most underestimated the $E1$ strength in the region under exam.

The $\Delta K = 0$ and $\Delta K = 1$ $E1$ strength distributions in ^{168}Er are plotted in Fig. 17. The strength is almost entirely concentrated in the upper part of the

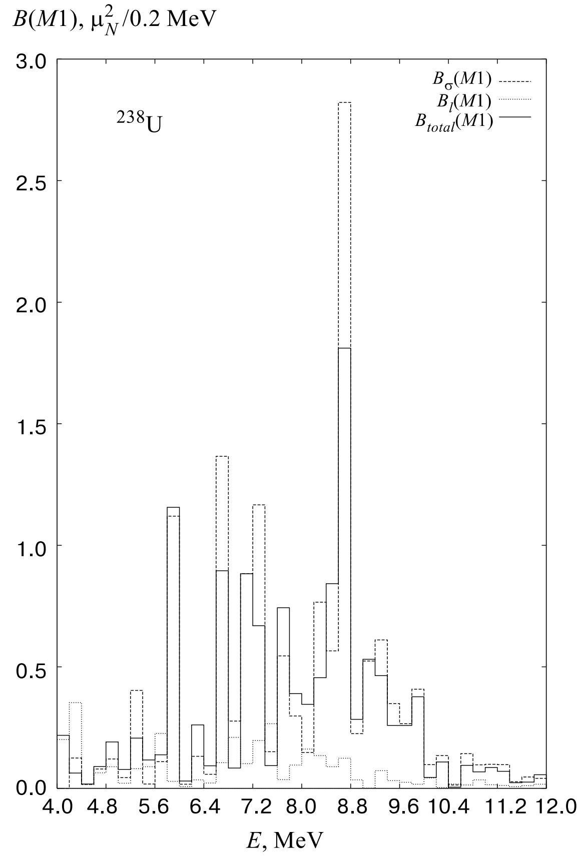

Fig. 16. The same as in Fig. 11 but for ^{238}U

spectrum, above ~ 6 MeV with a peak around ~ 7 MeV for both $\Delta K = 0$ and $\Delta K = 1$ transitions. An analogous spectrum was produced for ^{238}U (Fig. 18), where, however, some non-negligible strength occurs also in the low-energy region. The properties of the $E1$ spectra in this region are different from those of the low-lying levels. While, in fact, in the 2–4 MeV the $\Delta K = 0$ strengths are more than twice the $\Delta K = 1$ transition probabilities, in the region considered here, instead, the $\Delta K = 0$ and $\Delta K = 1$ strengths have similar distribution and comparable magnitude. The $\Delta K = 1$ $E1$ strength increases with the excitation energy more rapidly than the $\Delta K = 0$ one. According to our calculation, the running sums of the $\Delta K = 0$ and $\Delta K = 1$ $E1$ strengths become equal at 5.5 MeV in ^{154}Sm, at 4.5 MeV in ^{178}Hf and at 7 MeV in ^{168}Er and ^{238}U. This is an indication of the increasing role of the GDR with increasing energy. This

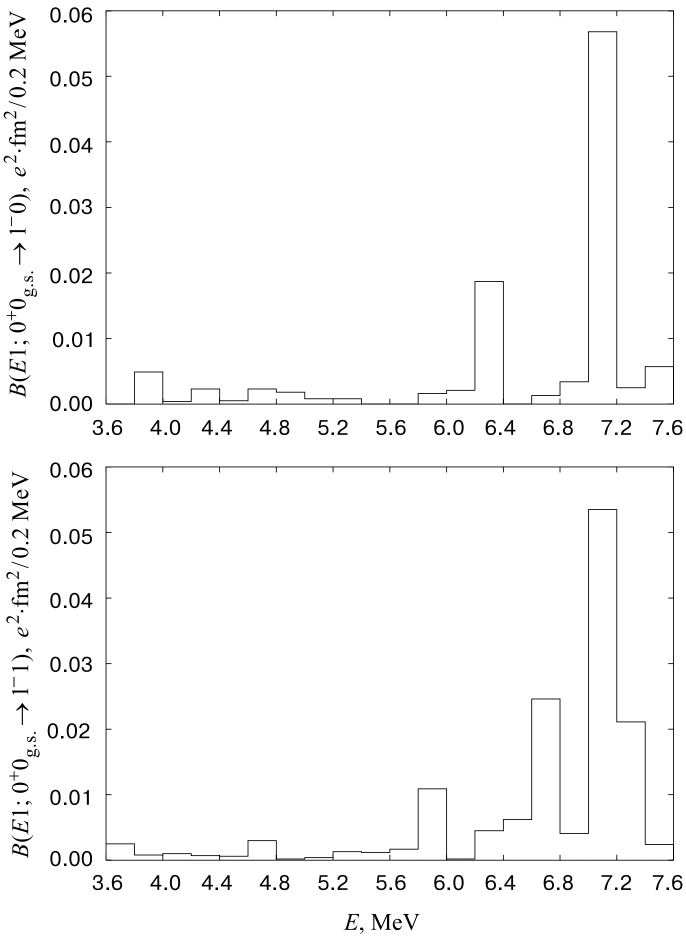

Fig. 17. $\Delta K = 0$ (upper part) and $\Delta K = 1$ (lower part) RPA $E1$ strength distributions, summed in bins of 0.2 MeV, are given for ^{168}Er in the 3.6–7.6 MeV energy range

point emerged more clearly when the $E1$ strength in ^{238}U was computed in the region 3.6–7.6 MeV. We got $\sum_i B(E1)\uparrow = 245 \cdot 10^{-3}$ e^{2}fm^2 for the $\Delta K = 0$ transitions and $\sum_i B(E1)\uparrow = 905 \cdot 10^{-3}$ e^{2}fm^2 for the $\Delta K = 1$ transitions. The comparison with the values obtained for the range 2.6–6.6 and shown in Table 12 indicates that above 6.6 MeV the onset of the giant dipole resonance takes place in ^{238}U.

4.4. Dipole Strength Distribution. Whenever the parity of the $I = 1$ states is unknown it is useful to give the dipole strength distribution as a sum of the $M1$ and $E1$ strengths. In order to make this sum consistently, we accounted for

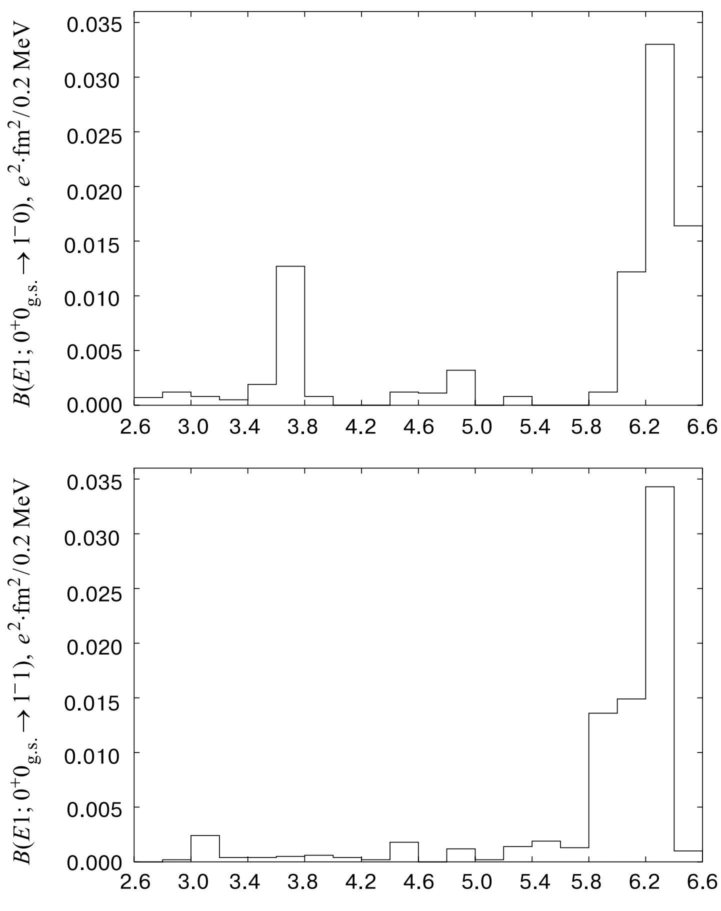

Fig. 18. RPA $\Delta K = 0$ (upper part) and $\Delta K = 1$ (lower part) $E1$ strength distributions are given for ^{238}U in the 2.6–6.6 MeV energy range

the fact that 1 $\mu_N^2 \approx 11 \cdot 10^{-3}$ e^{2}fm^2 and expressed the $B(M1)$ values in terms of 10^{-3} e^{2}fm^2 instead of μ_N^2. In this way the $B(E1)$ and $B(M1)$ values are both given in the units e^{2}fm^2. The $\Delta K = 0$ and $\Delta K = 1$ $E1$ strengths together with the $M1$ transition probabilities, both summed over the energy range 3.6–7.6 MeV for ^{154}Sm, ^{168}Er, and ^{178}Hf (2.6–6.6 MeV for ^{238}U) are given in Table 12. The total dipole sum is also given. One may notice that the total $E1$ strength is 3–4 times the summed $M1$ strength. This is in contrast to the low-energy region where $E1$ and $M1$ integrated strengths were comparable [10].

Table 12. $\Delta K = 0$ and $\Delta K = 1$ $E1$ strengths, $M1$ strengths and total $E1$ plus $M1$ strengths, summed over the 3.6–7.6 MeV range for ^{154}Sm, ^{168}Er, ^{178}Hf and over 2.6–6.6 MeV for ^{238}U

Nucleus	$\sum B(E1)\uparrow$ $\Delta K = 0$ $[10^{-3}\mathrm{e}^2\mathrm{fm}^2]$	$\sum B(E1)\uparrow$ $\Delta K = 1$ $[10^{-3}\mathrm{e}^2\mathrm{fm}^2]$	$\sum B(M1)\uparrow$ $[10^{-3}\mathrm{e}^2\mathrm{fm}^2]$	$\sum B_{\mathrm{total}}(E1)\uparrow + \sum B_{\mathrm{total}}(M1)\uparrow$ $[10^{-3}\mathrm{e}^2\mathrm{fm}^2]$
^{154}Sm	66	151	63	280
^{168}Er	107	142	58	307
^{178}Hf	121	150	79	350
^{238}U	137	171	66	374

The $B(M1)\uparrow$ and $B(E1)\uparrow$ values as well as their sum $B(M1)\uparrow + B(E1)\uparrow$, all in terms of $\mathrm{e}^2\mathrm{fm}^2$, are shown in Fig. 19 for ^{154}Sm and ^{168}Er. In both nuclei, the shape of the total dipole spectra differs considerably from the $E1$ or $M1$ dipole spectra. We still notice however that the position of the main peak is unchanged. The differences are even more marked in ^{178}Hf and ^{238}U is given in Fig. 20.

5. CONCLUSIONS

In conclusion, we can state the following:

1) The $K^\pi = 1^+$ states below 2 MeV in even–even nuclei are practically two-quasiparticle ones. Relevant experimental data are very scarce. For better understanding of a general situation with magnetic dipole excitations experimental measurement of the $M1$ and $E2$ transition rates for excitation of the $K^\pi = 1^+$ states below 2 MeV is needed.

2) The 1^+ states are orbital in the low-energy region. Fragmentation of the one-phonon strength affects the $M1$ strength distribution. An onset of fragmentation of the 1^+ states in actinides takes place at low excitation energies in comparison with ones in the rare-earth region. The quasiparticle–phonon interaction does not alter the global properties of the summed strength and its orbital nature. Fragmentation of the one-phonon states with $K^\pi = 0^-$ and 1^- strongly affects the $E1$ strength distribution at energies above 2.3 MeV. Generally, the calculated summed $B(E1)\uparrow$ strength for levels with $K^\pi = 0^-$ is three times as large as for the levels with $K^\pi = 1^-$ at energies below 2.5 MeV. Strong correlation takes place between $E1$ and $E3$ transition strengths.

3) The reduced transition widths $\Gamma_0^{\mathrm{red}}(M1)$ and $\Gamma_0^{\mathrm{red}}(E1)$ summed in the energy range 2–4 MeV are practically equal. Therefore, it is necessary to measure the parity of the $K = 1$ states.

4) Fast $E1$ and $M1$ transitions are expected between large components of the wave functions differing by the octupole with $K = 0$ or $K = 1$ and quadrupole with $K = 1$ phonon. It will be interesting to measure these fast γ-ray transition rates.

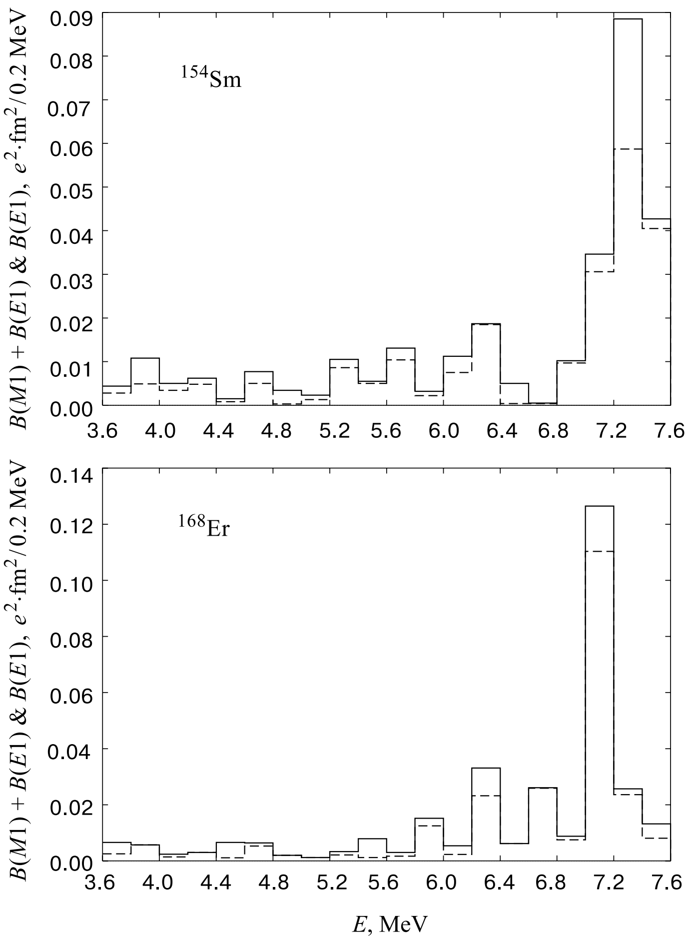

Fig. 19. The dipole distributions, $B(E1) + B(M1)$, summed in bins of 0.2 MeV, are given for ^{154}Sm (upper part) and ^{168}Er (lower part) in the 3.6–7.6 MeV energy range

5) Most of the $M1$ transitions in the energy range 2–4 MeV are of the orbital nature. The total $M1$ strength is larger than the sum of the orbital and spin parts. It means that the coherent coupling of the orbital and spin parts takes place in the energy range 2–4 MeV. The spin $M1$ strength dominates at energies above 6 MeV. It is found that the orbital motion, though giving on the whole a modest

contribution to the $M1$ strength, plays a significant role in shaping the $M1$ spectra because of the destructive interference between orbital and spin amplitudes.

6) Strong $E1$ transitions also occur in the same energy range. Their total strength in the energy range 3.6–7.6 MeV is about 4 times larger than the M1 strength. Because of these highly intense $E1$ transitions, the total dipole strength distribution computed as a sum of the $M1$ and $E1$ strengths is considerably different from the spectra of the $M1$ transitions alone.

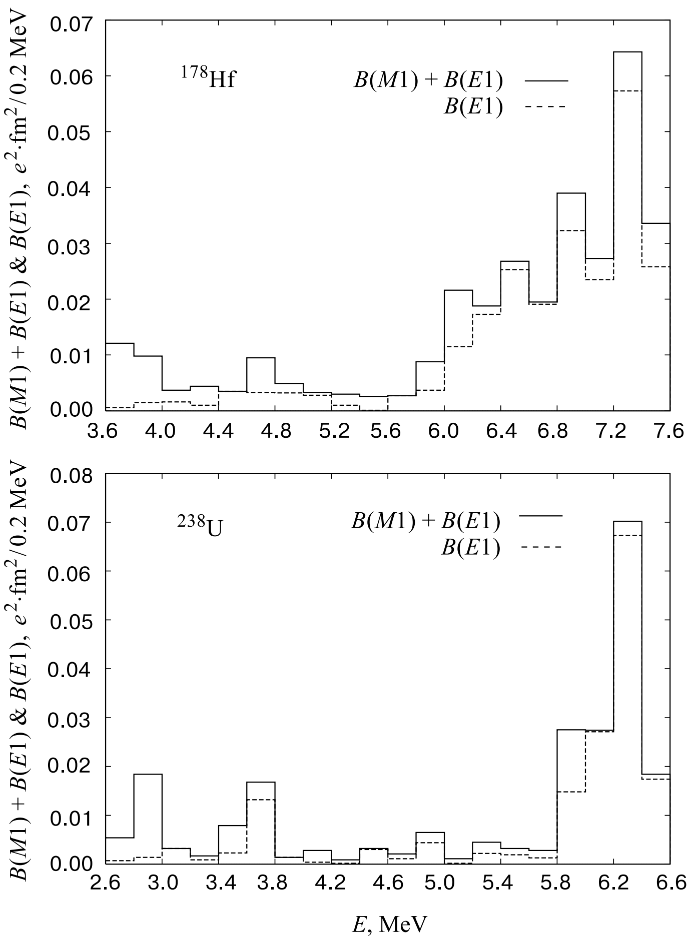

Fig. 20. The $B(E1)+B(M1)$ distributions, summed in bins of 0.2 MeV, are given for ^{178}Hf (upper part) in the 3.6–7.6 MeV energy range and for ^{238}U (lower part) in the 2.6–6.6 MeV region

We are grateful to N. Lo Iudice for fruitful cooperations, to U. Kneissl, P. von Neumann-Cosel and N. Pietrallo for valuable discussions and for sending the experimental data before publication, and P. von Brentano and R.D. Herzberg for useful discussions.

This review is written without V.G.Soloviev using the last common articles. A.V.Sushkov and N.Yu.Shirikova are very grateful to Professor V.G.Soloviev for the long fruitful cooperation, his great number of ideas and inexhaustible source of energy with which he had charged and still continues to charge us.

REFERENCES

1. **Bohle D., Richter A., Steffen W., Diepenrink A.E.L., Lo Iudice N., Palumbo F., Scholten O.** — Phys. Lett., 1984, v.B137, p.27.
2. **Lo Iudice N., Palumbo F.** — Phys. Rev. Lett., 1978, v.41, p.1532;
   De Franceschi G., Palumbo F., Lo Iudice N. — Phys. Rev., 1984, v.C29, p.1496.
3. **Richter A.** — Prog. Part. Nucl. Phys., 1995, v.34, p.261.
4. **Kneissl U., Pitz H.H., Zilges A.** — Prog. Part. Nucl. Phys., 1996, v.37, p.349.
5. **Lo Iudice N.** — Phys. Part. Nucl., 1997, v.28 p.556.
6. **Soloviev V.G.** — Theory of Atomic Nuclei: Quasiparticles and Phonons, Institute of Physics, Bristol and Philadelphia, 1992.
7. **Soloviev V.G., Sushkov A.V., Shirikova N.Yu.** — Phys. Part. Nucl., 1994, v.25, p.157
8. **Soloviev V.G., Sushkov A.V., Shirikova N. Yu., Lo Iudice N.** — Nucl. Phys., 1996, v.A600, p.155.
9. **Soloviev V.G., Sushkov A.V., Shirikova N.Yu.** — Z. Phys., 1997, v.A358, p.287.
10. **Soloviev V.G., Sushkov A.V., Shirikova N.Yu.** — Phys. Rev., 1997, v.C56, p.2528.
11. **Soloviev V.G., Sushkov A.V., Shirikova N.Yu.** — Int. J. Mod. Phys., 1994, v.E3, p.1227.
12. **Soloviev V.G., Sushkov A.V., Shirikova N.Yu.** — J. Phys. G, 1995, v.21, p.1217.
13. **Djalali C. et al.** — Phys. Lett., 1985, v.B164, p.269 .
14. **Frekers D. et al.** — Phys. Lett., 1989, v.B218, p.439.
15. **Frekers D. et al.** — Phys. Lett., 1990, v.B244, p.178.
16. **Richter A.** — Nucl. Phys., 1990, v.A507, p.99c; 1991, v.A522, p.139c.
17. **Richter A.** — The Building Blocks of Nuclear Structure, ed. A. Covello, Singapore, World Scientific, 1993, p.335.
18. **von Neumann-Cosel P.** — Prog. Part. Nucl. Phys., 1997, v.38, p.213.
19. **Soloviev V.G., Sushkov A.V., Shirikova N.Yu., Lo Iudice N.** — J. Phys. G, 1999, v.25, p.1023.
20. **Soloviev V.G., Sushkov A.V., Shirikova N.Yu.** — Phys. Atomic Nuclei, 1996, v.59, p.51.
21. **Gallagher G.J. Moszkowski S.A.** — Phys. Rev., 1958, v.111, p.1282.
22. **Soloviev V.G., Sushkov A.V., Shirikova N.Yu., Lo Iudice N.** — Nucl. Phys., 1997, v.A613, p.45.
23. **Nojarov R., Faessler A., Dingfelder M.** — Phys. Rev., 1995, v.C51, p.2449.

24. **Sarriguren P., Moya de Guerra E., Nojarov R.** — Phys. Rev., 1996, v.C54, p.690.
25. **Soloviev V.G., Sushkov A.V.** — Phys. Atomic Nuclei, 1994, v.57, p.1304.
26. **Hamamoto I.** — Nucl. Phys., 1973, v.A205, p.225; 1993, v.A557, p.515c.
27. **Maser H. et al.** — Phys. Rev., 1996, v.C53, p.2749.
28. **Nojarov R., Faessler A.** — Nucl. Phys., 1988, v.A484, p.1.
29. **Hamamoto I., Magnusson C.** — Phys. Lett., 1992, v.B312, p.267.
30. **Faessler A., Nojarov R., Taigel T.** — Nucl. Phys., 1989, v.A492, p.105.
31. **Lo Iudice N., Richter A.** — Phys. Lett., 1989, v.B304, p.193.
32. **Faessler A., Nojarov R., Scholz F.G.** — Nucl. Phys., 1990, v.A515, p.237.
33. **Zilges A., von Brentano P., Wesselborg C., Heil R.D., Kneissl U., Lindenstruth S., Pitz H.H., Seeman U., Stock R.** — Nucl. Phys., 1990, v.A507, p.399.
34. **Browne E.** — Nucl. Data Sheets, 1991, v.61, p.1.
35. **Freeman S.J. et al.** — Phys. Lett., 1989, v.B222, p.347.
36. **Freeman S.J. et al.** — Nucl. Phys., 1993, v.A552, p.10.
37. **Pietralla N. et al.** — Nucl. Phys., 1997, v.A618, p.141.
38. **Heil R.D., Pitz H.H., Berg U.E.P., Kneissl U., Hummel K.D., Kilgus G., Bohle D., Richter A., Wesselborg C., von Brentano P.** — Nucl. Phys., 1988, v.A476, p.39.
39. **Zilges A., von Brentano P., Herzberg R.D., Kneissl U., Margraf J., Piettalla N., Pitz H.H.** — Phys. Rev., 1995, v.C52, p.R468.
40. **McGowan F.K., Milner W.T.** — Nucl. Phys., 1994, v.A571, p.569.
41. **Soloviev V.G., Sushkov A.V., Shirikova N.Yu.** — Sov. J. Nucl. Phys., 1991, v.53, p.65.
42. **Klora J., Börner H.G., von Egidy T., Hiller H., Judge S., Khitrov V.A., Krushe B., Libman V.A., Linder H., Litvinski L.L., Mayerhofer U., Murzin A.V., Robinson S.J., Sukhovoj A.M.** — Nucl. Phys.. 1993, v.A561, p.1.
43. **Petkov P., Andrejtscheff W., Copnell J., Robinson S.J.** — Nucl. Phys., 1991, A533, p.49.
44. **Alessi J.G., Saladin J.X., Baktash C., Humanic T.** — Phys. Rev., 1981, v.C23, p.79.
45. **Rangacharyulu C., Richter A., Wörtche H.J., Ziegler W., Casten R.F.** — Phys. Rev., 1991, v.C43, p.R949.
46. **Soloviev V.G.** — Phys. Rev., 1995, v.C51, p.R2885.
47. **Pietralla N., von Brentano P., Hezberg R.D., Kneissl U., Margraf J., Maser H., Pitz H.H., Zilges A.** — Phys. Rev., 1995, v.C52, p.R2317.
48. **Soloviev V.G., Sushkov A.V., Shirikova N.Yu.** — Phys. Atomic Nuclei, 1997, v.60, p.10.
49. **Pitz H.H., Berg U.E.P., Heil R.D., Kneissl U., Stock R., Wesselborg C., von Brentano P.** — Nucl. Phys., 1989, v.A492, p.411.
50. **Friedrichs H. et al.** – Nucl. Phys., 1994, v.A567, p.266.
51. **Friedrichs H. et al.** — Phys. Rev., 1992, v.C45, p.R892.
52. **Margraf J. et al.** — Phys. Rev., 1995, v.C52, p.2429.